Aus der Klinik für Anästhesiologie m. S. operative Intensivmedizin der

Medizinischen Fakultät Charité – Universitätsmedizin Berlin

DISSERTATION

Stress-induced alterations in the organ systems during heart failure following an aortocaval fistula in rats

zur Erlangung des akademischen Grades

Doctor rerum medicinae

(Dr. rer. medic.)

vorgelegt der Medizinischen Fakultät Charité – Universitätsmedizin

Berlin von

Noureddin Bashir Aboryag

aus Alzawiyah/Libyen

Datum der Promotion: 06.03.2020

Table of Contents

1. Abstract

1.1 Abstract (English)

Heart and kidney are closely related during the course of heart failure. Indeed, a growing body of clinical data suggest that heart failure is a significant risk factor for kidney disease, which contributes to a higher mortality and morbidity. Unfortunately, until now the underlying mechanisms, which lead to the progressive renal damage during heart failure, are still lacking. Therefore, the main aim of this study was to investigate in male rats the effect of ACF-induced heart failure on hemodynamic parameters, kidney histology as well as on putative alterations in apoptotic factors responsible for apoptotic events during renal damage. The results showed that a significant increase in the weight indices of the heart and lung following ACF-induced heart failure was associated with systolic and diastolic dysfunction as reflected by significant changes in hemodynamic parameters compared to control. As a consequence of this ACF-induced heart failure, histological and ultrastructural alterations indicated obvious renal damage. Moreover, DNA fragmentation analysis showed a strong TUNEL positive staining in the nuclei of renal cells confirming an ongoing apoptotic process in the kidneys of rats with ACF-induced heart failure. Consistently, double immunofluorescence confocal microscopy showed proapoptotic Bax overexpression, mitochondrial leakage of cytochrome C into cell cytoplasm concomitant with the transfer of activated caspase 3 into to the nucleus of renal cells to initiate an apoptotic process. Taken together, these findings provide histological, immunohistochemical and ultrastructural evidence of an ongoing apoptotic process in the kidneys of rats with ACF-induced congestive heart failure supporting the notion that there is a pathological interaction between heart and kidney during heart failure.

1.2 Abstract (Deutsch)

Herz und Niere sind während des Herzversagens eng miteinander verbunden. In der Tat deuten immer mehr klinische Daten darauf hin, dass die Herzinsuffizienz ein signifikanter Risikofaktor für eine Nierendysfunktion ist, der zu einer höheren Mortalität und Morbidität beiträgt. Leider fehlen bis heute Erkenntnisse über die möglichen zugrundeliegenden Mechanismen, die zum progressiven Nierenschaden bei Herzinsuffizienz führen. Das Hauptziel dieser Studie war es daher, bei männlichen Ratten die Wirkung von ACF-induzierter Herzinsuffizienz auf hämodynamische Parameter, die Nierenhistologie sowie auf apoptotische Faktoren zu untersuchen, die an apoptotischen Ereignissen während einer Nierenschädigung beteiligt sind. Der signifikante Anstieg der Gewichtsindizes von Herz und Lunge nach ACF-induzierter Herzinsuffizienz war mit einer systolischen und diastolischen Dysfunktion verbunden, was sich im Vergleich zur Kontrolle durch signifikante Änderungen der hämodynamischen Parameter zeigte. Als Folge dieser ACF-induzierten Herzinsuffizienz wiesen histologische und ultrastrukturelle Veränderungen auf offensichtliche Nierenschäden hin. Darüber hinaus zeigte die DNA-Fragmentierungsanalyse eine starke TUNEL-positive Färbung in den Kernen von Nierenzellen, was einen anhaltenden apoptotischen Prozess in den Nieren von Ratten mit ACF-induzierter Herzinsuffizienz bestätigte. Konsequent zeigte die konfokale Doppelimmun-fluoreszenzmikroskopie eine proapoptotische Bax-Überexpression, einen mitochondrialen Austritt von Cytochrom C in das Zellcytoplasma und ein gleichzeitig erfolgter Transfer von aktivierter Caspase 3 in die Zellkerne der Nierenzellen, was einen apoptotischen Prozess initiiert. Zusammengenommen liefern diese Ergebnisse histologische, immunhistochemische und ultrastrukturelle Hinweise für einen fortlaufenden apoptotischen Prozess in den Nieren von Ratten mit ACF-induziertem kongestivem Herzversagen. Dies unterstreicht die pathologische Interaktion zwischen Herz und Niere im Rahmen einer Herzinsuffizienz.

2. Introduction

2.1 Heart failure and its consequences on the kidney

Heart failure is characterized by the inability of the heart to pump a sufficient amount of oxygenated blood to peripheral organs (Palazzuoli et al., 2016). As a consequence there is a mismatch between oxygen demand and delivery. In addition, this forward failure is accompanied by a backward failure, i.e. increased central venous pressure, organ congestion, and elevated abdominal pressure (Palazzuoli et al., 2016). All this amounts to organ dysfunction and finally injury, a scenario that is known for the kidney. Approximately one third of heart failure patients suffer from renal dysfunction (Palazzuoli et al., 2016; Ronco et al., 2008). Thus, heart performance and kidney function are closely interconnected and dysfunction of one organ may deteriorate the function of the other organ, a phenomenon commonly referred to as cardio-renal syndrome (Palazzuoli et al., 2016; Ronco et al., 2008). Indeed, impaired renal function is regarded as a crucial factor influencing the progress and prognosis of heart failure (Marenzi et al., 2007). Previous experimental studies have shown that – in addition to reduced organ perfusion - increased central and renal venous pressure leads to enhanced sodium retention and impaired glomerular filtration rate (Firth et al., 1988). In support of these observations, clinical trials have shown that increased central venous pressure in heart failure patients was closely associated with renal deterioration and disease prognosis (Damman et al., 2009). Earlier notion that hypervolemia and hyperperfusion of the kidney is beneficial for the renal function has been abandoned and the importance of the interstitial renal oedema leading to renal failure has received more attention (Prowle et al., 2014). However, a systematic histological analysis of the kidney during heart failure is lacking. This study addresses the absence of detailed histological, immunohistochemical and ultrastructural examinations of the kidney in cases of heart failure.

2.2 Animal model of ACF-induced heart failure

The experimental model of heart failure by volume overload *via* an aortocaval fistula was introduced first by Stumpe in 1971 (Stumpe et al., 1971). In this model an arteriovenous (AV) fistula between abdominal aorta and inferior vena cava is created by a longitudinal incision of both vessels and subsequent closure by use of a continuous Perlon suture No. 6 (MET). However, this model does take into account the knowledge that in the hands of a non-trained experimenter perioperative mortality is high and postoperative complications such as local haemorrhage is common and occurres quite often. Subsequently, the model of an aortocaval fistula was modified using a less invasive needle-technique in which an 18G needle was advanced from the aorta into the vena cava inferior at the site where both vessels appear to adhere to each other so that when the needle is withdrawn a shunt between aorta and vena cava remained (Garcia and Diebold et al., 1990). This modification resulted in congestive heart failure with a much-reduced risk of local bleeding; however, the development of heart failure lasted 8-10 weeks and was unpredictable (Garcia and Diebold et al., 1990; Brower GL, et al., 1996; Wang X et al., 2003). More recently, this model of infrarenal aortocaval fistula (ACF) was further improved by the use of 16G cannula, which had the advantage of producing congestive heart failure in a shorter period (28±2 days) and in a more predictable way (Treskatsch et al., 2014). In contrast to other models of heart failure (e.g. pressure overload) volume overload-induced heart failure leads to eccentric hypertrophy of the heart with an apparent dilation of the left ventricle with migration of various immune cells and apoptotic events as reported by Chen et al., 2011.

2.3 Apoptosis

Apoptosis is defined as programmed cell death, which is observed as cell shrinkage, nuclear fragmentation, chromatin condensation, and chromosomal DNA fragmentation (Tixeira et al., 2017). A human adult loses approximately 50 to 70 billion cells daily due to apoptosis (Elmore

2007). In contrast necrosis defines cell death due to acute cellular injury. Apoptosis is initiated by the intrinsic and extrinsic pathways. These two pathways converge at the mitochondrial outer membrane resulting in mitochondrial outer membrane permeabilization. The intrinsic pathway (mitochondrial apoptotic pathway) or suicidal pathway is triggered in response to intracellular stress such as calcium overload, oxidative stress and/or DNA damage. These events trigger the Bax/Bak-dependent mitochondrial outer membrane permeabilization and release of cytochrome C from mitochondria into cytosol (Alberts B et al., 2015). Cytosolic cytochrome C then forms apoptosomes leading to the activation of caspase 9 (entire pathway until DNA fragmentation).

In contrast, the extrinsic apoptosis is initiated by extracellular stress signals involving Fas ligand, tumour necrosis factor-α (TNF-α), and TNF-α-related apoptosis inducing ligand (TRAIL) through binding to their individual death receptors TNF-α receptor 1, Fas, and TRAIL receptor 1/2, respectively. Death receptors then recruit Fas-associated death domain and procaspase 8 into the death-inducing signalling complex, leading to caspase 8 activation. The activated initiator caspase 9 or 8 further induces activation of the effector caspases 3, 6, and 7, resulting in cleavage of essential cellular substrates and apoptosis (endpoint DNA fragmentation) (Peng Xia et al., 2016). Reports suggest heart failure may lead to apoptotic cell death in peripheral organs (e.g. liver) (Peter et al., 2000; Shaqura et al., 2017). For example, apoptosis has been observed in the heart (Peter et al., 2000) and involving peripheral organs affected by heart failure (Shaqura et al., 2017) in different animal models.

2.4 Objective or main hypothesis of the study

The aim of this study was to investigate the histopathological alterations and consequences of heart failure in peripheral organs such as kidney induced by an aortocaval fistula. Moreover, I investigated whether theses histopathological alterations were due to the occurrence of apoptotic events in peripheral organs such as the kidney.

3. Materials and Methods

3.1 Animals

All the experiments were performed in male Wister rats, weighing 280-300 g (Harlan Winkelmann, Borchen, Germany). The animals were kept on a 12 hours light- dark cycle at 23°C and 75% humidity with standard laboratory rat chow and water ad libitum in the animal facility of the Charité-Universitätsmedizin Berlin. This study followed the European Directive introducing new animal welfare and care guidelines recommendations (2010/63 / EU). Importantly, IRB approval for animal experiments was obtained by local authorities (LaGeSo, Berlin, Germany). All surgical procedures were performed under isofluran (ACF induction) or tiletamine/zolazepam (hemodynamic measurements) anaesthesia and all efforts were made to relief pain. Intra- and postoperative analgesia was provided by metamizole.

3.2 Experimental heart failure model

An 18G needle was used in experiments to induce an infrarenal aortocaval fistula (ACF) as previously described by Garcia and Diebold (Garcia and Diebold et al., 1990; Treskatsch et al., 2014). In a modified approach, a laparotomy was performed and then the aorta punctured with a 16G needle (Braun, Melsungen, Germany) distal to the renal arteries (Treskatsch et al., 2014). Afterwards, the needle was advanced through the aortic wall into the adjacent inferior vena cava. Following transient compression of the aorta and venous vessels above and below the puncture site, the needle was gently withdrawn and then the aortic puncture site sealed with a drop of cyanoacrylate adhesive. Immediately, blood shunting from the inferior aorta into the inferior vena cava was observed. When the animals were sacrificed after 28 ± 2 days of ACF-induced heart failure, the success of the aortocaval fistula (n=5 rats for morphometric/hemodynamic measurements, for immunohistochemistry and for electron microscopy, respectively) was visualized by the pulsatile flow of oxygen-enriched blood into the inferior vena cava from the infra renal aorta (Treskatsch et al., 2014; Dent et al., 2010). On

the other hand, sham operated rats (n=5 rats for morphometric/hemodynamic measurements, for immunohistochemistry and for electron microscopy, respectively) also received a laparotomy, with the vessels being temporarily compressed but without aortic puncture.

3.3 Morphometric data

After 28 ± 2 days of ACF-induced heart failure, the rats were sacrificed in isoflurane anaesthesia and blood, heart, lung and kidney tissues were rapidly removed. The wet weight of heart, lung and kidney tissues were measured by a balance (Sartorius TE6100 Talent Analytical Balance, 6100 g x 1 g. Sartorius Balances and Weighing Equipment.) and normalized to the body weight of the individual animal in order to calculate the respective indices (organ wet weight (mg)/ body weight (g))

3.4 Hemodynamic measurements

In order to perform hemodynamic measurements, we used spontaneously breathing rats to the closed-chest method as described in the previous studies (Treskatsch et al., 2014; Pacher et al., 2008). All measurements were performed under tiletamine/zolazepam anaesthesia (Zoletil®, 10 mg/kg s.c. followed by 50 mg/kg i.m.) 28 ± 2 days after fistula induction (Treskatsch et al., 2014; Saha et al., 2007). All data were recorded and analysed by the Power Lab®-system/-software (AD Instruments, New Zealand). In order to assess central venous pressure, a PE-50 tube catheter was inserted through the left jugular vein into the superior vena cava post tracheostomy. However, the arterial blood pressure was measured by cannulating the right carotid artery with a micro-tip pressure-volume conductance catheter (Millar®, SPR-838 NR). Additionally, the intraventricular pressures and volumes were assessed by advancing the catheter into the left ventricle and optimizing its position, aiming for maximum stroke volume (SV). To measure the parallel conductivity, 100 µl of 15% saline was injected into the central venous line as a correction factor for the blood-left ventricular (LV) tissue interface. Subsequently, the heart rate was obtained from the ECG signal. After hemodynamic

measurements were completed, animals were sacrificed by exsanguination and the organs were eviscerated for further determination.

3.5 Tissue preparation

Rats were deeply anesthetized with isoflurane and perfused with 100 ml 0.1 m PBS (pH 7.4) transcardially followed by 300 ml cold PBS containing 4% paraformaldehyde and 0.2% picric acid (pH 7.4; fixative solution) for light and fluorescence microscopy and with 4% paraformaldehyde/0.1% glutaraldehyde/0.2% picric acid solution (pH 7.4) for electron microscopy, respectively (Treskatsch et al., 2015). Subsequently, kidneys were quickly removed and the renal tissue postfixed for 90 min at 4° C in the fixative solution and cryo-protected overnight at 4° C in PBS containing 10% sucrose. Afterwards, the consecutive sections (6 µm thick) were prepared on cryostat and mounted onto gelatine-coated slides.

3.6 Histological examination

Kidney tissue sections were stained with haematoxylin-eosin as described previously (Mayer, 1981). For histological analysis, we captured random non-overlapping fields from the cortex-to-cortico-medullary regions of each stained kidney section using a 40× magnification lens by light microscopy (Zeiss Axioplan photomicroscope equipped with a digital camera).

3.7 Transmission electron microscope

The kidney tissue of 5 rats was processed for electron microscopy as reported previously (Treskatsch et al., 2015; Mousa et al., 2004). Briefly, small tissue pieces were post-fixed in 1% tannic acid (in 0.1 m PBS) and 1% osmium tetroxide solution (in 0.1 m PBS), then dehydrated in ethanol and finally embedded in Epon. Semithin and ultrathin sections were cut using a Reichert Ultracut (Leica, Germany) followed by contrast with 2% uranyl acetate / lead citrate. Finally, ultrathin sections were examined under a transmission electron microscope (TEM 10, Zeiss, Germany). Semithin sections were stained for 1 to 2 minutes in 1% Toluidine Blue

(Merck, Darmstadt, Germany), rinsed several times in purified water and examined under a light microscope (Axiophot 100, Zeiss, Germany).

3.8 Apoptosis Assay

Kidney apoptosis was measured by in situ terminal deoxynucleotidyl-transferase-mediated dUTP nick-end-labeling (TUNEL) assay using a commercially available kit (Chemicon Apo-Direct Tunel Assay Kit, Merck Millipore, Darmstadt, Germany) to detect internucleosomal DNA -fragmentation, indicating signs of apoptosis as per manufacturer's instructions. Briefly, paraformaldehyde-fixed kidney tissue sections (6 μm) with pre-cooled fixative (ethanol / acetic acid) were placed at -20 ° C for 5 minutes. These were then washed with PBS wash and the tissue sections immersed in 1xTdT equilibration buffer at room temperature for 30 minutes followed by incubation with TdT enzyme activity for 1 hour at 37 ° C. The reaction was terminated with working strength stop/wash buffer and the sections washed with PBS. Subsequently, the tissue sections were incubated for 30 minutes at room temperature on FITC-conjugated anti-digoxigenin. Following the PBS wash, the nuclei were stained bright blue with 4'-6-diamidino-2-phenylindole (DAPI) (0.1 μg / ml in PBS) (Sigma). For negative control, kidney tissue sections were incubated in the absence of TdT enzyme.

3.9 Double-immunofluorescence staining

The double immunofluorescent staining of mitochondrial marker for cytochrome C in the kidney was performed as reported previously (Mousa et al., 2016; Shaqura et al., 2016). Briefly, non-specific binding was blocked with blocking solution containing 10% bovine serum albumin and 5% donkey serum. Then, kidney sections were incubated overnight with the primary antibodies: 1) monoclonal mouse anti-mitochondria (Cat MA5-12017, Thermo Fisher Scientific, Rockford, IL) in combination with rabbit polyclonal anti-cytochrome C (cat #4280, Cell Signalling, Danvers, MA; 2) rabbit polyclonal anti-cleaved caspase 3 (cat # 9661, cell signalling), anti-caspase 3 (cat # ab13847, Abcam, Cambridge, MA) and anti-Bax protein (cat

SC-526, Santa Cruz biotechnology, Texas). After incubation with primary antibodies, the tissue sections were washed with PBS three times for 60 minutes and then incubated with red fluorescent Alexa Fluor 594 donkey anti-rabbit secondary antibody (Vector Laboratories) in combination with green fluorescent Alexa Fluor 488 donkey anti-mouse antibody (Invitrogen, Germany) for 120 minutes. This was followed by PBS wash and the nuclei stained blue with 4'-6 Diamidino-2-phenylindole (DAPI) (0.1 µg/ml in PBS) (Sigma).

3.10 Quantification of immunostaining

Quantification of immunofluorescent co-localization of mitochondrial marker with cytochrome C in kidney tissue sections was performed using the Zeiss Zen 2009 software Carl Zeiss Micro-Imaging GmbH (Göttingen, Germany) as described previously (Shaqura et al., 2016; Manders et al., 1993). The co-localization of proteins of interest was quantified by calculating the co-localization coefficient based on Pearson's correlation coefficient as reported previously (Manders et al., 1993). In order to exclude background fluorescence, the images were adjusted to the threshold and then gated to include only the intensity measurements from positively stained cells. The number of caspase-3 stained nuclei was determined by the formula: caspase-3 stained nuclei/total number of DAPI stained nuclei ×100. The images analysis was performed using area of the whole stained tissue section. Data were expressed as means ± S.E.M.

3.11 Statistical analysis

All the hemodynamic parameters were analyzed using SPSS 20.0 software program. The Kolmogorov-Smirnov test was used to analyze the normal distribution. All the parameters were expressed as means ± SEM. Statistical significance between two groups was analyzed by student t-test or Mann-Whitney U test where appropriate. $P<0.05$ was considered statistically significant. All morphological parameters were analyzed by Sigma Plot 13.0 statistical software.

4. Results

4.1 Increased heart and lung weight indices in ACF rats

The wet weight of the hearts (2402 ± 299.7 mg) and lungs (2756 ± 511.2 mg) were significantly greater in rats with ACF-induced heart failure compared to controls (hearts: 1400 ± 99.8 mg; lungs: 1390 ± 86.0 mg) ($p<0.01$). However, the body weight of rats with ACF-induced heart failure (352.2 ± 40.5 mg) were not significantly different from sham operated control animals (361,2 ± 23,1) (**Fig. 1**) . As a consequence heart and lung weight indices (heart/lung wet weight (mg) body weight (g) were significantly higher in rats with ACF-induced heart failure (heart: 6.55 ± 0.56 mg/g; lung 7.54 ± 1.50 mg/g) than in controls (heart: 3.92 ± 0.18 mg/g; lung 3.90 ± 0.37 mg/g).

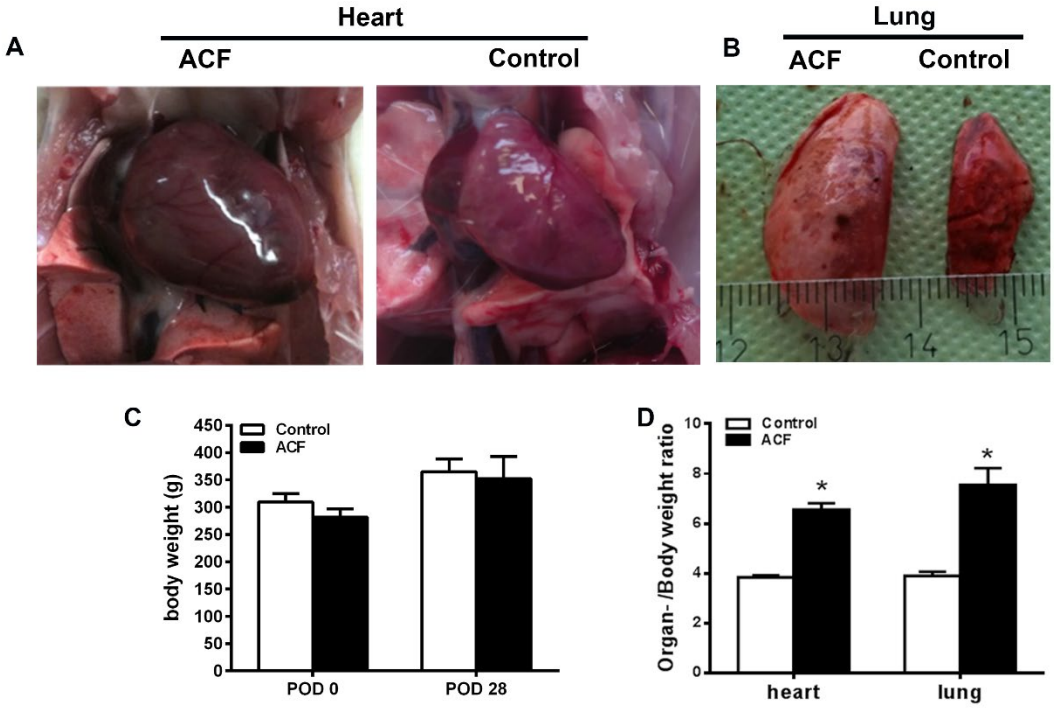

Figure 1: Heart and lung enlargements and increased wet weights in rats with ACF-induced heart failure. A, B) Photographs of the hearts and lungs of rats with ACF-induced heart failure show greatly enlarged and congested organs compared to sham operated rats; **C**) The body weight of the two groups of animals were not significantly different, whereas (**D**) the heart and lung ratios were significantly increased in rats with ACF-induced heart failure. ($p<0.05$, student t-test). Figure 1 is obtained from Aboryag et al. 2017, Oxidative Medicine and Cellular Longevity, article ID 6894040)

4.2 Systolic and diastolic dysfunction in rats with ACF-induced heart failure

In vivo measurements of different hemodynamic parameters in ACF rats compared to controls revealed that the central venous pressure (CVP) and left end-diastolic pressure (LVEDP) were significantly higher in ACF rats compared to controls ($p<0.05$) (**Table 1**). In addition, the left ventricular end-diastolic and end-systolic volumes (LVEDV, LVESV) were significantly increased ($p<0.05$) in ACF rats compared to controls. Moreover, the left ventricular ejection fraction (LVEF) was significantly reduced ($p<0.05$) (**Table 1**).

Table 1: Hemodynamic parameters

	Control (n=5)	**ACF (n=5)**
SV (µl)	134±3	298±40*
LVEF (%)	74±2	45±4*
LVEDP (mmHg)	5.1±0.3	12.1±1*
ZVD (mmHg)	0.1±0.1	5.6±1*
HR (min^{-1})	340.41±10	316.98±10
LVESV (µl)	48.18±5	359.71±36*
LVEDV (µl)	181.86±8	658.04±61*

Data are expressed as means ± s.e.m. Two-tailed student t-test: * denotes *P<0.05* for comparisons with control

4.3 Histopathological changes in the kidney in rats with ACF-induced heart failure

The haematoxylin-eosin and toluidine blue staining of kidney tissue sections of control rats demonstrated a normal histological structure of glomeruli, proximal and distal tubule **(Fig. 2A** and **Fig. 4B)**. However, the microscopic analyses of kidney tissue sections of rats with ACF-induced heart failure revealed signs of morphological and pathological alterations**:** i) in the

glomerular region of the kidney, many glomeruli lost their prominent glomerular structure such as widening of Bowman's space with obvious degenerations of cells with pyknotic nuclei and the presence of cell remnants **(Fig. 2C, D)**; ii) the proximal convoluted tubules (PCT) revealed various atrophic changes such as epithelial shedding as well as obvious losses of brush borders **(Fig. 2C, D)**; iii) within the tubular regions of kidneys there were desquamated epithelia cells, tubular cell destructions with obvious degenerations of nuclei, and signs of apoptotic cell deaths (pyknotic nuclei) **(Fig. 2C, D)**; iv) tubular lumens of various tubules became obliterated due to degenerations and swelling of lining epithelial cells **(Fig. 2C, D)**.

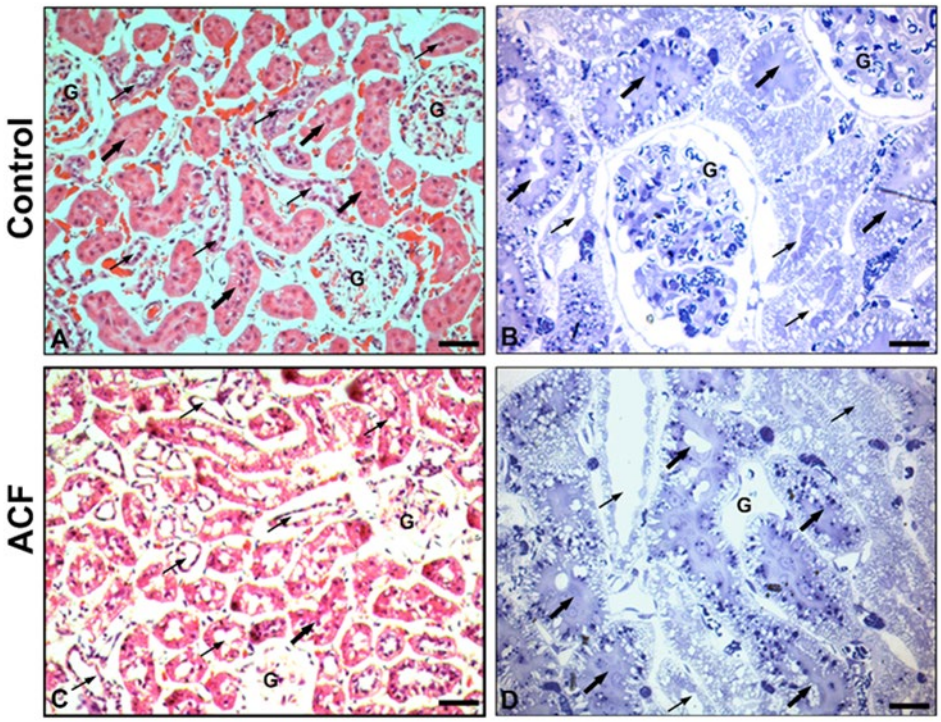

Figure 2: Light microscopic photographs of kidneys from control and ACF rats. (A, B) show control haematoxylin-eosin (**A**) and toluidine blue (**B**) stained rat kidney sections with normal distal (thin arrow), proximal (thick arrow) tubular and glomerular (G) structures. **(C, D)** show ACF haematoxylin-eosin (**C**) and toluidine blue (**D**) stained rat kidney sections with histopathological changes in atrophic glomeruli (**D**) as widening of Bowman's space with haemolysis, obvious degenerations of nuclei and apoptotic cell deaths. Moreover, histopathological changes in atrophic distal (thin arrow) and proximal (thick arrow) tubular structures (**D**) reveal epithelial shedding and loss of brush borders of proximal tubules as well as desquamation of tubular epithelium of distal tubules in the medulla. A, C: x120; B, D: x200.

4.4 Detection of DNA fragmentation by TUNEL staining in kidney cells of rats with ACF-induced heart failure

Evidence of apoptotic cell death in kidneys of ACF-rats and the degree of DNA fragmentation was assessed by TUNEL staining. Immunofluorescent analyses demonstrated fragmented DNA strands in numerous tubular epithelial cells of ACF rats visualized by staining with the fluorochrome FITC-conjugated anti-digoxigenin green in close proximity of DAPI-positive nuclei (**Fig. 3C, D**). In contrast, TUNEL-positive cells were not detected in control rats (**Fig. 3A, B**).

4.5 Upregulation of proapoptotic Bax expression in kidney cells of rats with ACF-induced heart failure

Confirmation of TUNEL staining observations and to assess the possible mechanisms of renal cell apoptosis the apoptotic factor immunoreactivity in kidney, sections of rats with ACF-induced heart failure were examined using double immunofluorescence confocal microscopy. Proapoptotic Bax protein immunofluorescent staining was faintly observed in the proximal and distal tubules with absence of staining in the glomeruli or interstitium of control rats **(Fig. 3E, F)**. However, ACF-induced heart failure was associated with significantly upregulated Bax immunoreactivity in the damaged proximal and distal tubular cells of kidney tissue sections (**Fig. 3G, H**). Moreover, various glomerular cells showed strong Bax immunostaining **(Fig. 3G, H**).

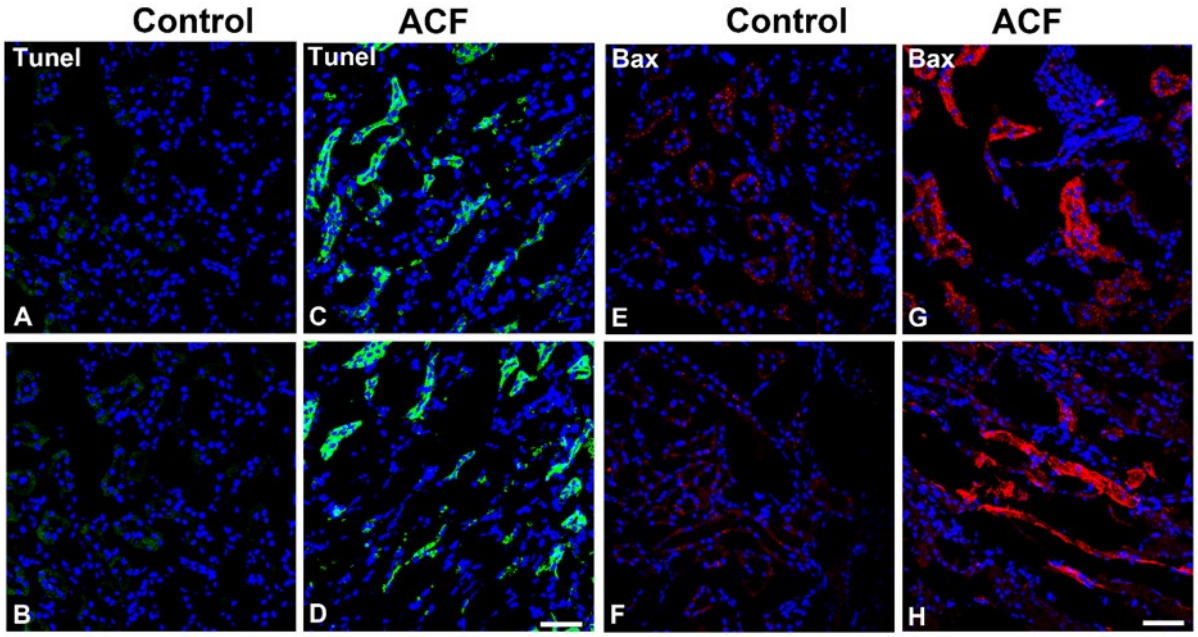

Figure 3: Immunofluorescence confocal microscopy of TUNEL staining (A-D) or of proapoptotic Bax protein (E-H) in kidney sections of control compared to ACF-rats. (**A-D**) show TUNEL-positive (green fluorescence) with DAPI-counterstained nuclei (blue fluorescence) immunofluorescence of kidney sections of control (**A, B**) or ACF (**C, D**) rats. Note the apoptotic TUNEL-ir tubular cells in kidney sections following ACF-induced heart failure (**C, D**), however, no TUNEL staining was found in control animals **(A, B**). **(E-H)** demonstrate proapoptotic Bax protein immunoreactivity (red fluorescence) with DAPI-counterstained nuclei (blue fluorescence) of kidney sections of control (**E, F**) or ACF (**G, H**) rats. Note that only absent or weak Bax immunostaining was detected in the renal tubular cell cytoplasm of control kidneys (**E, F**). However, strong positive immunofluorescence staining was found within renal tubular cell cytoplasm in ACF rats (**G, H**). Bar=20 µm.

4.6 Mitochondrial leakage of cytochrome C into the cytosol of kidney cells of rats with ACF-induced heart failure

Putative leakage of the enzyme cytochrome C from mitochondria of renal cells indicating apoptotic cell death during heart failure was also assessed. Double immunofluorescence confocal microscopy revealed that cytochrome C immunoreactivity was predominantly localized to mitochondria within renal tubular cells of control rats indicated by an almost complete overlap with a highly specific mitochondrial marker (a 60kDa non-glycosylated protein component of mitochondria) **(Fig. 4)**. On the other hand, cytochrome C immunoreactivity apparently leaked from mitochondria of renal tubular cells of ACF rats and

expanded mostly into the cytoplasm, predominantly in the perinuclear area. In parallel, cytochrome C was no longer colocalized with the mitochondrial marker **(Fig. 4)**. The quantitative analysis of the colocalization coefficient of cytochrome C and mitochondrial marker within renal tissue sections demonstrated a significant decrease of their colocalization in ACF animals compared to controls indicating that cytochrome C had leaked from mitochondria into the cytoplasm **(Fig. 6)**.

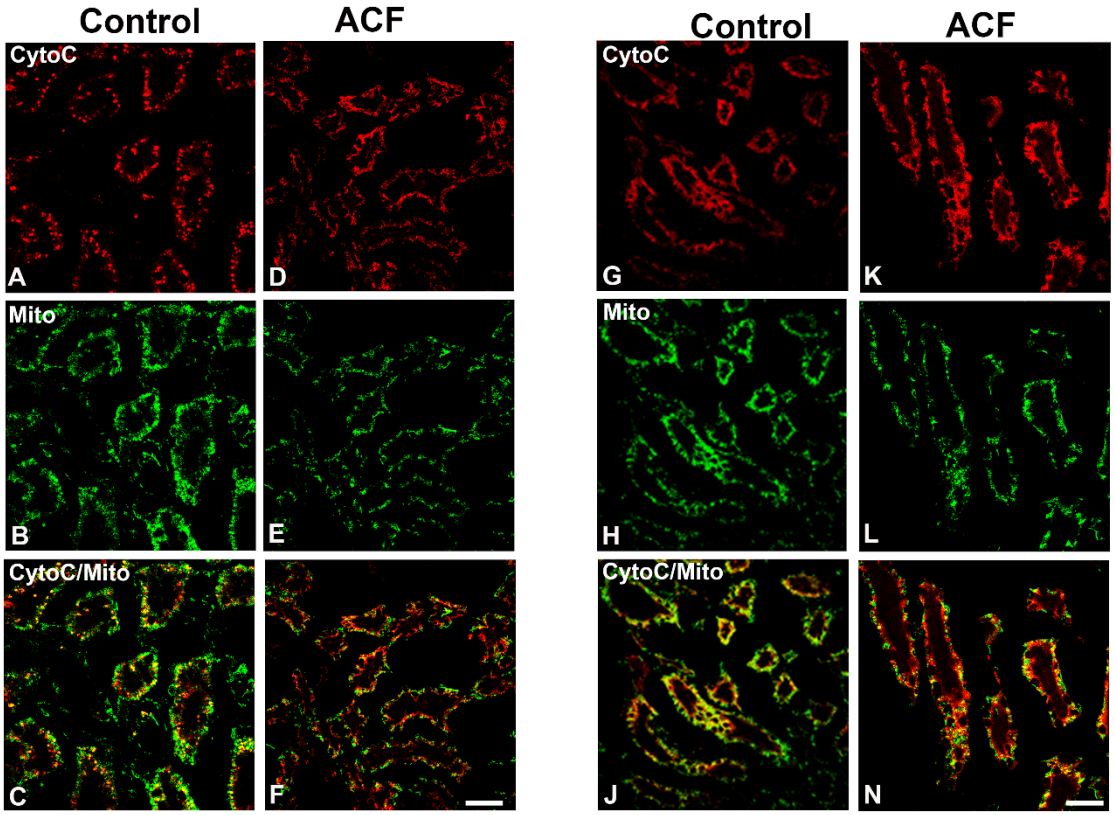

Figure 4: Double immunofluorescence confocal microscopy of cytochrome C (red fluorescence) with mitochondrial marker (green fluorescence) double immunofluorescence of the renal tubular cells in the kidney of control and ACF rats. Note that the cytochrome C immunostaining overlapped with the mitochondrial marker in the cytoplasm of renal tubular cells of control kidneys (**A-C, G-J**). However, cytochrome C immunofluorescence was distributed primarily within the cytoplasm after heart failure induction, where it no longer colocalized with mitochondria within renal tubular cells (**D-F, K-N**). Bar=20 µm.

4.7 Nuclear transfer of caspase 3 as activated caspase 3 in kidney cells of rats with ACF-induced heart failure

To further corroborate the evidence for apoptotic pathway-mediated renal cell death, morphological evidence for the presence of caspase 3 and its activated form from cell organelle-like structures in renal tubules and glomerular cells of ACF rats was assessed. In control animals, kidney sections showed that caspase 3 immunoreactivity was restricted predominantly to well define subcellular structures in proximal and distal tubular cells with absence of staining in the glomeruli or interstitium **(Fig. 5A, B)**. However, in ACF rats, caspase 3 immunoreactivity was translocated into perinuclear area of cells or nuclei within tubular cells of the kidney **(Fig. 5C, D)**. In addition, various glomerular cells exhibited a positive immunostaining suggesting caspase 3 had been activated **(Fig. 5C, D)**. Therefore, we used cleaved activated caspase-3 as an apoptotic marker which is absent under normal conditions and easily detectable during cell apoptosis. Using an antibody, which detects cleaved caspase 3 recombinant protein in kidney sections of ACF rats, these results demonstrate that the cleaved caspase 3 immunoreactivity was confined primarily to the perinuclear area of cells or nuclei within tubular cells (**Fig. 5G, H**). Moreover, the number of caspase-3-IR nuclei as well as cleaved caspase-3-IR nuclei cells in relation to the total number of DAPI stained nuclei was significantly increased in ACF rats compared to the controls ($P<0.05$) (**Fig. 6B**).

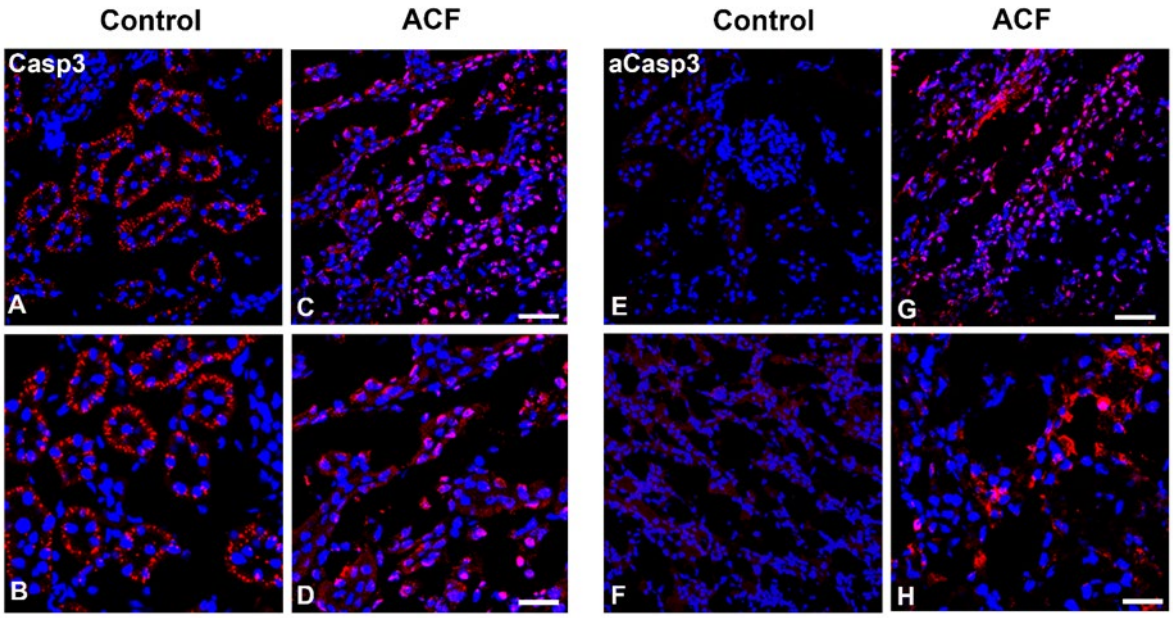

Figure 5: Confocal immunofluorescence microscopy of caspase 3 (red fluorescence) using an antibody detecting pro-caspase 3 recombinant protein (A-D) or activated (cleaved) caspase 3 recombinant protein (E-H) with DAPI-counterstained nuclei (blue fluorescence) in kidney sections of control or ACF rats. (**A-D**) Note, caspase 3 immunoreactivity was confined primarily to well define subcellular organelle-like structures in renal tubular cells within kidney sections of control rats. In contrast in ACF rats, caspase-3 immunofluorescence was transferred into the perinuclear area of cells or inside the nuclei of renal tubular cells (**C** and **D**) indicating an activation of proapoptotic factor caspase 3. (**E-H**) Confocal immunofluorescence microscopy of activated caspase-3 (red fluorescence) and DAPI-counterstained nuclei (blue fluorescence) in kidney sections using an antibody detecting exclusively cleaved caspase 3 recombinant protein. (**G, H**) showed that cleaved caspase-3 immunoreactivity was confined primarily to the perinuclear area of cells or nuclei within renal tubular (**G**) and glomerular (**H**) cells of ACF rat kidneys, however, no staining was found in control animals (**E, F**). Bar=20 µm.

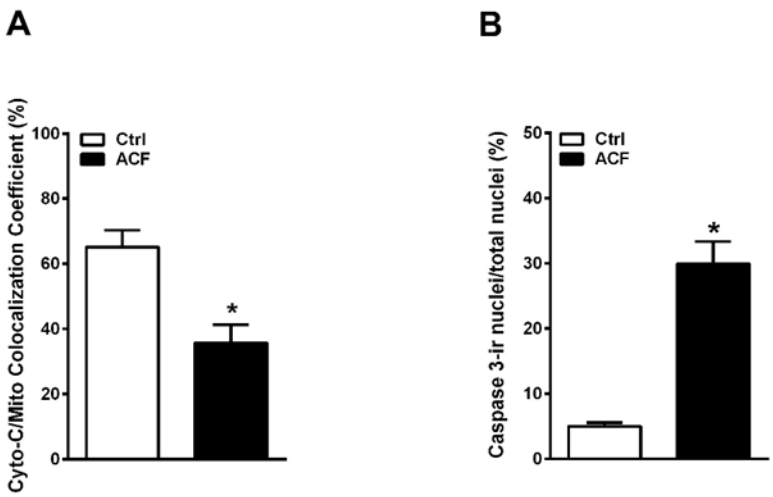

Figure 6: (A) Quantitative analysis of immunofluorescence confocal microscopy of mitochondrial leakage of cytochrome C into the cytosol as well as of the nuclear transfer of activated caspase 3 into the nucleus of kidney cells of ACF rats. Quantitative analysis of immunofluorescence microscopy of the colocalization coefficient of cytochrome C and the mitochondrial marker showing a significant reduction of their colocalization in the kidney of ACF animals compared to controls ($P<0.05$, student t-test). (**B**) Quantitative analysis of immunofluorescence microscopy for cleaved caspase-3-IR renal tubular cell nuclei in the kidney of ACF animals relative to controls ($P<0.05$, student t-test). Data are expressed as means ± s.e.m.

4.8 Ultrastructural pathological changes in kidney cells of rats with ACF-induced heart failure

Ultrastructural examination of renal sections of control rats stained with uranyl acetate and lead citrate revealed normal renal cell structure with normal mitochondria and endoplasmic reticulum (**Fig. 7A**). In contrast, kidney sections from ACF rats showed the following pathological signs: obvious cytoplasmic vacuolization of cells, dilated endoplasmic reticulum, enlarged mitochondria and pleomorphic lysosomes containing flocculent material (**Fig. 7B, C**). Moreover, the ultrastructural changes in the renal glomeruli and tubular cells of ACF kidneys included signs of matrix vacuolization, blood capillary dilation and nuclei degeneration (**Fig. 7B, C**. In addition, the space between individual tubules were enlarged and there was a prominent capillary dilation in the peritubular area within oedematous regions (**Fig. 7B**). The renal tubules exhibited various ultrastructural changes such as numerous swollen mitochondria with a cristae disarrangement and partial cristalysis of tubular epithelium (**Fig. 7 C)**.

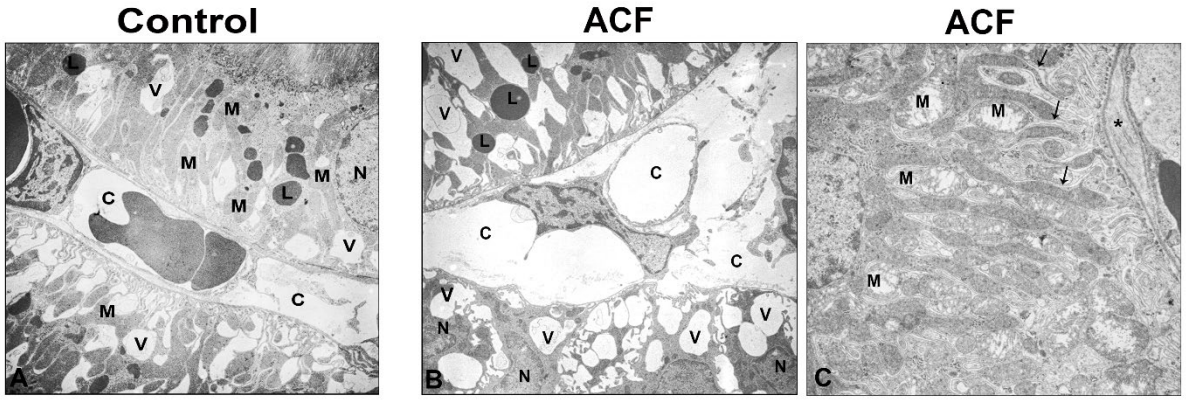

Figure 7: Transmission electron micrographs of the rat kidney in control (A) and ACF (B and C) rats. (**A**) shows a normal ultrastructure of control kidney cells. Note, normal kidney cells consisted of vital nuclei (N), well-developed cell organelles, mitochondria (M), lysosomes (L) and a well-organized cytoplasm. (**B**) Electron microscopic demonstration of the ACF kidney tissue. Note, ultrastructure evaluations showed a marked cytoplasmic vacuolization (V) of cells, capillary (C) dilation in the peritubular area, dilated cell organelles and cell nuclei (N) became condensed indicating intrinsic apoptotic events. (**C**) Many swollen mitochondria situated between the extensive inholdings (arrow) of the basolateral plasma membrane (*) that create the lateral cell processes of distal tubules which are dilated and exhibit a cristae disarrangement and partial cristolysis. x5000; Bars:1 µm.

5. Discussion

Introducing an infrarenal aortocaval shunt in rats by the modified 18G-needle technique (Treskatsch et al., 2015) resulted in typical signs of high-output congestive heart failure, i.e. increased left ventricular end-diastolic and end-systolic volumes, elevated central venous pressure and left end-diastolic pressure as well as a reduced left ventricular ejection fraction. Consequently, heart and lung indices were significantly increased compared to controls which indicates a transition from eccentric hypertrophy with preserved cardiac function to severe biventricular dilatation with decompensated heart failure (Treskatsch et al., 2015). Consistent with these observations, previous studies using this animal model have shown that rBNP plasma concentrations increased almost 4-fold (Treskatsch et al., 2015), an established biomarker for heart failure. Moreover, reduced expression of ß1- and ß2-adrenoreceptors in this animal model

provide indirect evidence for an enhanced activation of the sympathetic nervous system (Treskatsch et al., 2015).

It has been previously reported that impaired cardiac output causes impaired renal perfusion and increased venous pressure leading to reduced glomerular filtration rate and acute kidney injury (Ronco et al., 2008). Under chronic conditions of heart failure, excessive sympathetic activation, increased oxidative stress to kidney, and impaired nitric oxide function on the renal vascular endothelium may lead to severe kidney injury (Ronco et al., 2008). However, there is scant evidence regarding the precise histomorphological alterations and their putative mechanisms of heart failure-induced kidney injury. This study aimed to assess the histo-morphological evidence for the heart failure-induced kidney damage.

In line with the above-mentioned hemodynamic consequences of ACF-induced heart failure and a reduced kidney perfusion as well as the increased venous congestion, a number of renal histopathological alterations were observed in kidney sections stained with haematoxylin-eosin or toluidine blue. The changes observed included: glomerular atrophy with widening of Bowman's space, epithelial shedding into the tubular lumen, nuclei pyknosis (chromatin condensation in the nucleus), desquamated cells as well as local haemorrhages suggesting the occurrence of apoptotic events. These apoptotic events in renal tissue were confirmed by demonstrating DNA fragmentation by TUNEL assay. Strong TUNEL positive staining was detected in numerous glomerular and tubular renal cells consistent with apoptotic events in the kidney of rats with ACF-induced heart failure. Similarly, tubular cell apoptosis in rat kidneys was observed following left coronary artery-induced myocardial infarction (Cho et al., 2013).

Other reports have stated that the activation of pro-apoptotic protein Bax leads to the disruption of the mitochondrial transmembrane potential, mitochondrial swelling and increased permeability of the outer mitochondrial membrane resulting in the release of cytochrome C (Green, 2000; Deng et al., 2008). In keeping with these observations, immunofluorescent confocal microscopy revealed proapoptotic Bax overexpression in kidney tubular cells

following ACF-induced heart failure. Moreover, double immunofluorescence confocal microscopy analysis showed that cytochrome C leaked into the cytosol of renal tubular epithelial cells but was not co-localized with mitochondria following ACF-induced heart failure. These findings support previous studies demonstrating cytochrome C release from mitochondria into the cytosol following cadmium treatment to trigger caspase activation in isolated kidney cortex (Lee et al., 2004). Similarly, the present results are consistent with reported data suggesting cytochrome C release from mitochondria to the cytosol during apoptotic events in kidney of rats with hypertensive nephron-sclerosis (Ying and Sanders, 2001).

Evidence for apoptotic events triggering renal cell death was further substantiated by the demonstration of activation of caspase 3 and subsequent translocation of its cleaved form from cell organelle like structures into the perinuclear area of renal tubular epithelial and glomerular cells of rats with ACF-induced heart failure. These observations provide further evidence in support of published data showing the activation of caspase 3 in cisplatin-induced renal injuries (Kaushal et al., 2001) and polymyxin-induced apoptosis in rat kidney proximal tubular cells (Azad et al., 2015).

Finally, electron microscopy analysis confirmed the presence of renal cell apoptosis as reflected by signs of nuclear condensation, DNA fragmentation and shrinkage as well as dissolution of mitochondrial structure. These findings are in agreement with the growing body of clinical data suggesting that heart performance and kidney function are closely interconnected and imply close links between these two organs (Fonarow et al., 2005). Moreover, Yancy et al. stated that the dysfunction of either heart or kidney often leads to a deterioration of function of the other one (Yancy et al., 2013). Recently, an investigation of acute renal injury reported that cell death, inflammation, cytokine and chemokine overexpression, caspase-mediated apoptotic mechanisms and oxidative stress might induce distant organ dysfunction (Li et al., 2014; Bang et al., 2005).

In summary, a growing body of clinical data indicated that heart failure often triggers kidney's injury a phenomenon called cardio-renal syndrome (Bongartz, 2005). The present findings showed that the progressive heart failure (Treskatsch et al., 2015) is accompanied with a significant increase in the weight indices of the heart and lung concomitant with systolic and diastolic dysfunction. In parallel, there are apoptotic events associated with nucleus degeneration, mitochondrial swelling and cell death in the glomerular and tubular area of the kidney. Moreover, the overexpression of pro-apoptotic Bax protein concomitant with cytochrome C release from the outer mitochondrial membrane into cell cytoplasm led to subsequent caspase 3 activation triggering apoptotic events following ACF-induced heart failure. Overall, these observations provide evidence of apoptotic processes that may mediate renal damage due to congestive heart failure and support the notion that there is a pathological interaction between heart and kidney during heart disease.

6. References

Alberts B, Johnson A, Lewis J, Raff M, Roberts K, Walter P."Chapter 18 Apoptosis: Programmed Cell Death Eliminates Unwanted Cells". Molecular Biology of the Cell (textbook) (5th ed.) Garland Science. 2008 p. 1115. ISBN 978-0-8153-4105-5.

Bang, Gniadecki R, Gajkowska B. Disruption of lipid rafts causes apoptotic cell death in HaCaT keratinocytes. Exp Dermatol Apr, 2005; vol. 14, no. 4, pp. 266-72.

Bongartz LG, Cramer MJ, Doevendans PA, Joles JA, Braam B. The severe cardiorenal syndrome: 'Guyton revisited', Eur Heart J. Jan, 2005; 26:11-7.

Brower GL, Henegar JR, Janicki JS.Temporal evaluation of left ventricular remodelling and function in rats with chronic volume overload.Am J Physiol. Nov, 1996; 271: H2071-8.

Chen YW, Pat B, Gladden JD, Zheng J, Powell P, Wei CC, Cui X, Husain A, Dell'italia LJ. Dynamic molecular and histopathological changes in the extracellular matrix and inflammation in the transition to heart failure in isolated volume overload. Am J Physiol Heart Circ Physiol. 2011; 300: H2251-60.

Cho E, Kim M, Ko YS, Lee HY, Song M, Kim MG, Kim HK, Cho WY, Jo SK. Role of inflammation in the pathogenesis of cardiorenal syndrome in a rat myocardial infarction model. Nephrol Dial Transplant. Nov, 2013; 28:2766-78.

Damman K, van Deursen VM, Navis G, Voors AA, van Veldhuisen DJ, Hillege HL. Increased central venous pressure is associated with impaired renal function and mortality in a broad spectrum of patients with cardiovascular disease.J Am Coll Cardiol. Feb, 2009;17;53:582-588.

Deng J, Wang G, Huang Q, Yan Y, Li K, Tan W, Jin C, Wang Y, Liu J. Oxidative stress-induced leaky sarcoplasmic reticulum underlying acute heart failure in severe burn trauma. Free Radic Biol Med. Feb, 2008;44: 375-85.

Dent MR, Tappia PS, Dhalla NS. Gender differences in cardiac dysfunction and remodelling due to volume overload. J Card Fail. May, 2010; 16: 439-49.

Elmore S. Apoptosis: a review of programmed cell death. Toxicol Pathol. Jun, 2007; 35: 495-516.

Firth JD, Raine AE, Ledingham JG. Raised venous pressure: a direct cause of renal sodium retention in oedema?. Lancet May ,1988; 7;1:1033-5.

Fonarow GC, Adams KF Jr, Abraham WT, Yancy CW, Boscardin WJ. Risk stratification for in-hospital mortality in acutely decompensated heart failure: classification and regression tree analysis. JAMA Feb, 2005;293:572-80.

Garcia R1, Diebold S. Simple, rapid, and effective method of producing aortocaval shunts in the rat. Cardiovasc Res May,1990;24:430-2.

Green DR, Apoptotic pathways: paper wraps stone blunts scissors, Cell, vol. Jul , 2000;102:1-4.

Heywood JT. The cardiorenal syndrome: lessons from the ADHERE database and treatment options, Heart Fail Rev. Jul, 2004;9:195-201.

Kaushal GP, Kaushal V, Hong X, Shah SV. Role and regulation of activation of caspases in cisplatin-induced injury to renal tubular epithelial cells. Kidney Int Nov,2001;60:1726-36.

Lee WK, Bork U, Thevenod F. Mitochondria as a target of cadmium nephrotoxicity: induction of swelling and cytochrome C release, Toxicol Mech Methods 2004;14:67-71.

Li CP, Li JH, He SY, Li P, Zhong XL**.** Roles of Fas/Fasl, Bcl-2/Bax, and Caspase-8 in rat nonalcoholic fatty liver disease pathogenesis. Genet Mol Res, May, 2014;13:3991-9.

Marenzi G1, Moltrasio M, Assanelli E, Lauri G, Marana I, Grazi M, Rubino M, De Metrio M, Veglia F, Bartorelli AL. Impact of cardiac and renal dysfunction on inhospital morbidity and mortality of patients with acute myocardial infarction undergoing primary angioplasty. Am Heart J. May ,2007;153:755-62.

Manders EM, Verbeek FG and Aten JA. Measurement of colocalization of objects in dual-colour confocal images, J Microsc Oxford. 1993;169:375-382.

Mousa SA, Shakibaei M, Sitte N, Schäfer M, Stein C. Subcellular pathways of beta-endorphin synthesis, processing, and release from immunocytes in inflammatory pain, Endocrinology. Mar, 2004;145:1331-41.

Mousa SA, Shaqura M, Winkler J, Khalefa BI, Al-Madol MA, Shakibaei M, Schulz S, Schäfer M. Protein kinase C-mediated mu-opioid receptor phosphorylation and desensitization in rats, and its prevention during early diabetes, Pain. Apr, 2016;157:910-21.

Palazzuoli A, Lombardi C, Ruocco G, Padeletti M, Nuti R, Metra M, Ronco C. Chronic kidney disease and worsening renal function in acute heart failure: different phenotypes with similar prognostic impact? Eur Heart J Acute Cardiovasc Care. Dec, 2016;5:534-548.

Pacher P, Nagayama T, Mukhopadhyay P, Bátkai S, Kass DA. Measurement of cardiac function using pressure-volume conductance catheter technique in mice and rats. Nat Protoc 2008;3:1422-34.

Peter M. Kang, Seigo. IzumoApoptosis and Heart FailureA Critical Review of the Literature American Heart Association, Inc.Circ Res. 2000;86:1107–1113.

Prowle JR, Kirwan CJ, Bellomo R. Fluid management for the prevention and attenuation of acute kidney injury.Nat Rev Nephrol. Jan, 2014;10:37-47.

Ronco C, House AA, Haapio M. Cardiorenal syndrome: refining the definition of a complex symbiosis gone wrong. Intensive Care Med May, 2008;34:957-62.

Saha DC, Saha AC, Malik G, Astiz ME, Rackow EC. Comparison of cardiovascular effects of tiletamine-zolazepam, pentobarbital, and ketamine-xylazine in male rats. J Am Assoc Lab Anim Sci Mar, 2007;46:74-80.

Shaqura M, Li X, Al-Khrasani M Shakibaei M, Tafelski S, Fürst S, Beyer A, Kawata M, Schäfer M, Mousa SA. Membrane-bound glucocorticoid receptors on distinct nociceptive

neurons as potential targets for pain control through rapid non-genomic effects. Neuropharmacology 2016;111 :1-13.

Shaqura M, Mohamed DM, Aboryag NB, Bedewi L, Dehe L, Treskatsch S, Shakibaei M, Schäfer M, Mousa SA. Pathological alterations in liver injury following congestive heart failure induced by volume overload in rats.PLoS One. Sep, 2017;12:e0184161.

Stump KO, Small H, Ressel C, Cruck Q. Increased Liquid resorption in superficial nephrons of Rats with generalized oedema due to aortocavalAnastomosis, VIII Symposium Society for Nephrology,edited by HEINTZ R, HOLZHUTER H, Aachen, Germany,September 1971, 1972, p. 23-25

Tixeira R, Caruso S, Paone S, Baxter AA, Atkin-Smith GK, Hulett MD, Poon IK "Defining the morphologic features and products of cell disassembly during apoptosis". Apoptosis. March 2017;22 : 475–477.

Treskatsch S, Feldheiser A, Rosin AT, Sifringer M, Habazettl H, Mousa SA, Shakibaei M, Schäfer M, Spies CD. A modified approach to induce predictable congestive heart failure by volume overload in rats," PLoS One. 2014;9:e87531.

Treskatsch S, Shakibaei M, Feldheiser A, Shaqura M, Dehe L, Roepke TK, Spies C, Schäfer M, Mousa SA. Ultrastructural changes associated with myocardial apoptosis, in failing rat hearts induced by volume overload. Int J Cardiol Oct, 2015;197:327-32.

Wang X, Ren B, Liu S, Sentex E, Tappia PS, Dhalla NS. Characterization of cardiac hypertrophy and heart failure due to volume overload in the rat. J Appl Physiol 2003;94: 752–763 .

Yancy CW, Jessup M, Bozkurt B , Butler J, Casey DE Jr, Drazner MH, Fonarow GC, Geraci SA, Horwich T, Januzzi JL, Johnson MR, Kasper EK, Levy WC, Masoudi FA, McBride PE, McMurray JJ, Mitchell JE, Peterson PN, Riegel B, Sam F, Stevenson LW, Tang WH, Tsai EJ, Wilkoff BL . ACCF/AHA guideline for the management of heart failure: a report of the American College of Cardiology Foundation/American Heart Association Task Force on Practice Guidelines, J Am Coll Cardiol. Oct , 2013;62:e147-239.

Ying WZ, and Sanders PW. Cytochrome C mediates apoptosis in hypertensive nephrosclerosis in Dahl/Rapp rats. Kidney Int 2001; 59: 662-72.

7. Declaration of individual contribution to the following publication:

Noureddin B. Aboryag, Doaa M. Mohamed, Lukas Dehe, Mohammed Shaqura, Sacha Treskatsch, Mehdi Shakibaei, Michael Schäfer, and Shaaban A. Mousa. Histopathological Changes in the Kidney following Congestive Heart Failure by Volume Overload in Rats. Oxidative Medicine and Cellular Longevity, 2017;2017:6894040. https://doi.org/10.1155/2017/6894040.

Noureddin B. Aboryag contributed to the concept and study protocol of the experiments. He prepared the animals for the experiments and performed under the supervision of Dr. L. Dehe and Prof. S. Treskatsch all surgical and interventional procedures necessary for the animal model of infrarenal aortocaval fistula (ACF). In addition, he was mainly responsible for sacrificing the animals to obtain blood, heart, lung and kidney, and he participated in the hemodynamic parameter assessments (Fig. 1., Table 1). He has performed immuno-histochemical experiments under the supervision of Dr. Shaaban Mousa (Fig. 2, 3, 4, 5, 6) and has helped Prof. Shakibaei with the electron microscopy (Fig. 7). He analyzed the respective results obtained from his experiments and wrote part of the methods and results section. Finally, he contributed to the introduction and discussion of the manuscript, revised the final draft and approved the final version of the manuscript.

Unterschrift, Datum und Stempel des betreuenden Hochschullehrers

_____

Prof. Dr. med. Michael Schäfer

Unterschrift des Doktoranden

_____

Noureddin B. Aboryag

8. Journal Data Filtered By Selected JCR Year: 2017 Selected Editions: SCIE, SSCI Selected Categories: "CELL BIOLOGY" Selected Category Scheme: WoS

Rank	Full Journal Title	Total Cites	Journal Impact Factor	Eigenfactor Score
1	NATURE REVIEWS MOLECULAR CELL BIOLOGY	43,667	35.612	0.095540
2	NATURE MEDICINE	75,461	32.621	0.171980
3	CELL	230,625	31.398	0.583260
4	Cell Stem Cell	23,493	23.290	0.096030
5	CANCER CELL	35,217	22.844	0.096910
6	Cell Metabolism	29,834	20.565	0.101740
7	NATURE CELL BIOLOGY	39,896	19.064	0.092960
8	TRENDS IN CELL BIOLOGY	13,708	18.564	0.037630
9	Science Translational Medicine	26,691	16.710	0.126450
10	CELL RESEARCH	13,728	15.393	0.037450
11	MOLECULAR CELL	61,604	14.248	0.181170
12	NATURE STRUCTURAL & MOLECULAR BIOLOGY	27,547	13.333	0.081820
13	Autophagy	14,923	11.100	0.035510
14	TRENDS IN MOLECULAR MEDICINE	9,213	11.021	0.019720
15	EMBO JOURNAL	67,036	10.557	0.079780
16	CURRENT OPINION IN CELL BIOLOGY	13,339	10.015	0.027790
17	DEVELOPMENTAL CELL	26,896	9.616	0.074980
18	GENES & DEVELOPMENT	57,469	9.462	0.092720
19	CURRENT BIOLOGY	56,595	9.251	0.137200

20	Cold Spring Harbor Perspectives in Biology	13,275	9.247	0.049360
21	Annual Review of Cell and Developmental Biology	9,812	9.032	0.016870
22	Cell Systems	1,129	8.982	0.009600
23	AGEING RESEARCH REVIEWS	5,297	8.973	0.012030
24	JOURNAL OF CELL BIOLOGY	68,915	8.784	0.085170
25	EMBO REPORTS	13,293	8.749	0.031350
26	PLANT CELL	48,393	8.228	0.063640
27	MATRIX BIOLOGY	4,803	8.136	0.008500
28	Cell Reports	29,789	8.032	0.210690
29	CELL DEATH AND DIFFERENTIATION	18,865	8.000	0.031540
30	AGING CELL	8,067	7.627	0.018910
31	CURRENT OPINION IN STRUCTURAL BIOLOGY	10,619	7.179	0.024320
32	ONCOGENE	66,411	6.854	0.075960
33	CELLULAR AND MOLECULAR LIFE SCIENCES	23,341	6.721	0.041340
34	Stem Cell Reports	4,525	6.537	0.026290
35	CYTOKINE & GROWTH FACTOR REVIEWS	5,668	6.395	0.008050
36	Science Signaling	10,316	6.378	0.037220
37	Protein & Cell	2,363	6.228	0.008060
38	SEMINARS IN CELL & DEVELOPMENTAL BIOLOGY	9,024	6.138	0.024200
39	Pigment Cell & Melanoma Research	4,430	6.115	0.007840
40	Wiley Interdisciplinary Reviews-RNA	2,142	5.844	0.009350
41	Cell Death & Disease	14,475	5.638	0.046010
42	FASEB JOURNAL	41,572	5.595	0.051640

42	Journal of Molecular Cell Biology	1,877	5.595	0.005920
44	STEM CELLS	21,694	5.587	0.035680
45	CELLULAR PHYSIOLOGY AND BIOCHEMISTRY	11,234	5.500	0.017450
46	Cell Communication and Signaling	2,034	5.324	0.005510
47	JOURNAL OF MOLECULAR AND CELLULAR CARDIOLOGY	14,186	5.296	0.025030
48	Aging-US	4,410	5.179	0.010910
49	CURRENT OPINION IN GENETICS & DEVELOPMENT	7,791	4.995	0.018550
51	Stem Cell Research & Therapy	4,578	4.963	0.012630
52	CELL PROLIFERATION	2,663	4.936	0.003440
52	Oxidative Medicine and Cellular Longevity	9,180	4.936	0.022930
54	STRUCTURE	14,417	4.907	0.036760
55	Cells	1,005	4.829	0.004100
56	CELLULAR ONCOLOGY	1,322	4.761	0.002020

9. Manuscript of the publication

Hindawi
Oxidative Medicine and Cellular Longevity
Volume 2017, Article ID 6894040, 10 pages
https://doi.org/10.1155/2017/6894040

Research Article

Histopathological Changes in the Kidney following Congestive Heart Failure by Volume Overload in Rats

Noureddin B. Aboryag,[1] Doaa M. Mohamed,[1] Lukas Dehe,[1] Mohammed Shaqura,[1] Sacha Treskatsch,[1] Mehdi Shakibaei,[2] Michael Schäfer,[1] and Shaaban A. Mousa[1]

[1]*Department of Anaesthesiology and Intensive Care Medicine, Charité University Berlin, Campus Virchow Klinikum and Campus Charité Mitte, Berlin, Germany*
[2]*Department of Anatomy, Ludwig-Maximilians-University Munich, Munich, Germany*

Correspondence should be addressed to Shaaban A. Mousa; shaaban.mousa@charite.de

Received 22 February 2017; Revised 7 April 2017; Accepted 2 May 2017; Published 31 July 2017

Academic Editor: Sidhartha D. Ray

Background. This study investigated histopathological changes and apoptotic factors that may be involved in the renal damage caused by congestive heart failure in a rat model of infrarenal aortocaval fistula (ACF). *Methods*. Heart failure was induced using a modified approach of ACF in male Wistar rats. Sham-operated controls and ACF rats were characterized by their morphometric and hemodynamic parameters and investigated for their histopathological, ultrastructural, and apoptotic factor changes in the kidney. *Results*. ACF-induced heart failure is associated with histopathological signs of congestion and glomerular and tubular atrophy, as well as nuclear and cellular degeneration in the kidney. In parallel, overexpression of proapoptotic Bax protein, release of cytochrome C from the outer mitochondrial membrane into cell cytoplasm, and nuclear transfer of activated caspase 3 indicate apoptotic events. This was confirmed by electron microscopic findings of apoptotic signs in the kidney such as swollen mitochondria and degenerated nuclei in renal tubular cells. *Conclusions*. This study provides morphological evidence of renal injury during heart failure which may be due to caspase-mediated apoptosis via overexpression of proapoptotic Bax protein, subsequent mitochondrial cytochrome C release, and final nuclear transfer of activated caspase 3, supporting the notion of a cardiorenal syndrome.

1. Introduction

Heart failure, a progressive disease marked by repeated hospitalizations for episodes of acute decompensation, is frequently complicated by kidney dysfunction—one of the most important risk factors for poor clinical outcome and death [1]. In congestive heart failure, the heart cannot deliver oxygen at a rate proportionate to the demands of the metabolizing tissues that may result in damage to other organ systems such as the kidney [2–4]. It is well established that heart performance and kidney function are closely interconnected and dysfunction of one organ often leads to a deterioration of the function of another which is known as cardiorenal syndrome [5]. Consistently, more than 1 million patients present to hospitals in the United States with acutely decompensated heart failure every year and approximately one-third of these patients develop kidney injury [6]. Consequently, these patients who develop kidney dysfunction after heart failure have a significantly higher mortality rate [7, 8]. In addition, there is emerging evidence that heart failure can also be considered as an inflammatory state that contributes to gradual toxic injury to renal cells including apoptosis which may lead to chronic kidney damage and functional loss [5, 9, 10]. Recently, Cho et al. showed that the number of TUNEL-positive apoptotic tubular cells significantly increased in the kidneys of rats with myocardial infarction [11].

Once cells receive the apoptotic stimulus, they constitute specific pathways, including the disruption of mitochondrial

transmembrane potential, followed by the release of mitochondrial proteins like cytochrome C and the activation of caspase subtypes within the apoptosome complex leading to cell death [12–14]. Recent evidence is emerging that the mitochondria-mediated apoptosis is initiated by a variety of apoptosis-inducing signals that cause the imbalance of the major apoptosis regulator such as Bcl-2 and Bax [15]. Therefore, the aim of our current study was to investigate the histopathological and ultrastructural changes in the kidney in a modified experimental rat model of infrarenal aortocaval fistula-induced heart failure. Moreover, we investigated possible alterations in the expression of apoptotic factors such as bax protein, cytochrome C, and caspase-3 as well as activated caspase-3.

2. Materials and Methods

2.1. Animals. Male Wistar rats, 280–300 g (Harlan Winkelmann, Borchen, Germany), were maintained on standard laboratory rat chow and water ad libitum. The animals were kept on a 12 h light–dark cycle with a temperature of 23°C and a humidity of 75%. This study was carried out in accordance with the European directive introducing new animal welfare and care guidelines (2010/63/EU). IRB approval for animal experiments was obtained from local authorities (Landesamt für Gesundheit und Soziales, Berlin, Germany). Surgical procedures were performed under isoflurane (ACF induction) and tiletamine/zolazepam (hemodynamic measurements) anesthesia, and all efforts were made to minimize suffering. Postsurgical analgesia was provided by metamizole (40 mg/kg s.c.).

2.2. Experimental Heart Failure Model. The needle technique to induce an infrarenal aortocaval fistula (ACF) has previously been described by Garcia and Diebold using an 18G needle [16, 17]. In a modified approach, a laparotomy was performed and the aorta was punctured by using a 16G needle (Braun, Melsungen, Germany) distal to the renal arteries [17]. Then, the needle was advanced through the aortic wall into the adjacent inferior vena cava. After temporarily compressing the aorta and venous vessels above and below the puncture site, the needle was carefully withdrawn and the aortic puncture site sealed with a drop of cyanoacrylate glue. Patency of the fistula ($n = 5$ rats for morphometric/hemodynamic measurements, for immunohistochemistry and for electron microscopy, resp.) was visualized by the pulsatile flow of oxygenated blood into the vena cava inferior from the infrarenal aorta [17, 18]. Sham-operated rats ($n = 5$ rats for morphometric/hemodynamic measurements, for immunohistochemistry and for electron microscopy, resp.) also received a laparotomy with the vessels temporarily compressed, but without any puncture of the aorta.

2.3. Morphometric Data. After 28 ± 2 days of fistula induction, the animals were sacrificed in isoflurane anesthesia and blood, heart, lung, and kidney tissues were quickly removed. The wet weight of heart, lung, and kidney tissues ($n = 5$ rats) was measured by a balance and normalized to the body weight of the individual animal to obtain the respective indices.

2.4. Hemodynamic Measurements. For hemodynamic measurements, the "closed chest" method in spontaneously breathing rats was used as described previously [17, 19]. All measurements were performed under tiletamine/zolazepam anesthesia (Zoletil®, 10 mg/kg s.c. followed by 50 mg/kg i.m.) 28 ± 2 days after fistula induction [17, 20]. Measurements were registered and analyzed by the PowerLab® system/software (AD Instruments, New Zealand). After tracheotomy, a PE-50-tubing catheter was inserted via the left jugular vein into the superior vena cava for the assessment of central venous pressure. Arterial blood pressure was measured by cannulating the right carotid artery with a microtip pressure-volume conductance catheter (Millar®, SPR-838 NR). Intraventricular pressures and volumes were registered by further advancing the catheter into the left ventricle and optimizing its position aiming for maximal stroke volume (SV). For measurement of the parallel conductance volume, 100 μl of 15% saline was injected into the central venous line as a correction factor for the blood-left ventricle (LV) tissue interface. Heart rate was derived from the ECG signal. After completion of the hemodynamic measurements, animals ($n = 5$ rats per group) were killed by exsanguination and organs were eviscerated for further determinations.

2.5. Tissue Preparation. Rats were deeply anesthetized with isoflurane and perfused transcardially with 100 ml 0.1 m PBS (pH 7.4) and 300 ml cold PBS containing 4% paraformaldehyde and 0.2% picric acid (pH 7.4; fixative solution) for light and fluorescence microscopy and with 4% paraformaldehyde/0.1% glutaraldehyde/0.2% picric acid solution (pH 7.4) for electron microscopy, respectively [21]. The kidneys were removed, renal tissue postfixed for 90 min at 4°C in the fixative solution, and cryoprotected overnight at 4°C in PBS containing 10% sucrose. Consecutive sections (6 μm thick) prepared on cryostat were mounted onto gelatin-coated slides.

2.6. Histological Examination. Kidney tissue sections from 5 rats were stained with hematoxylin and eosin as previously described [22]. For histological analysis, random nonoverlapping fields from the cortex-to-corticomedullary region of each kidney section were captured using a 40x magnification lens by light microscopy (Zeiss Axioplan photomicroscope equipped with a digital camera).

2.7. Transmission Electron Microscopy. Tissue of the kidney from 5 rats was processed for electron microscopy as described previously [21, 23]. Small pieces of tissue were postfixed in 1% tannic acid (in 0.1 m PBS) and 1% osmium tetroxide solution (in 0.1 m PBS), dehydrated in ethanol, and embedded in Epon. Semithin and ultrathin sections were cut on a Reichert Ultracut (Leica, Germany), followed by contrasting with 2% uranyl acetate/lead citrate. Finally, ultrathin sections were examined under a transmission electron microscope (TEM 10, Zeiss, Germany). Semithin sections were stained 1 to 2 minutes in 1% Toluidine Blue (Merck, Darmstadt, Germany), rinsed several times in

purified water, and examined under a light microscope (Axiophot 100; Zeiss, Germany).

3. Apoptosis Assay

The assessment of liver apoptosis was performed in situ using terminal deoxynucleotidyl transferase-mediated dUTP nick end-labeling (TUNEL) assays (Chemicon Apo-Direct Tunel Assay Kit; Merck Millipore, Darmstadt, Germany) for the detection of the internucleosomal DNA fragmentation, characteristic for apoptosis according to the manufacturer's instructions. Briefly, 6 μm sections of paraformaldehyde-fixed liver tissue were postfixed with precooled fixative (ethanol/acetic acid) for 5 min at −20°C. After PBS wash, the sections were then immersed in 1x TdT equilibration buffer at room temperature for 30 min followed by incubation with working strength TdT enzyme for 1 h at 37°C. The reaction was terminated with working strength stop/wash buffer, and the sections were washed with PBS. Then, the sections were incubated with FITC conjugated anti-digoxigenin at room temp for 30 min. After PBS washing, the nuclei were stained bright blue with 4′-6-diamidino-2-phenylindole (DAPI) (0.1 μg/ml in PBS) (Sigma). As a negative control, sections were incubated in the absence of TdT enzyme.

3.1. Double Immunofluorescence Staining. Double immunofluorescence staining of cytochrome C in the kidney was performed as described previously [24, 25]. Kidney sections were incubated overnight with the following primary antibodies: (1) monoclonal mouse anti-mitochondria (catalogue number MA5-12017, Thermo Fisher Scientific, Rockford, IL) in combination with rabbit polyclonal anti-cytochrome C (catalogue number 4280, Cell Signalling, Danvers, MA); (2) rabbit polyclonal anti-cleaved caspase-3 (catalogue number 9661, Cell Signalling), anti-caspase-3 (catalogue number ab13847, Abcam; Cambridge, MA), and anti-Bax protein (catalogue number SC-526, Santa Cruz Biotechnology, Texas). After incubation with primary antibodies, the tissue sections were washed with PBS and then incubated with red fluorescent Alexa Fluor 594 donkey anti-rabbit antibody (Vector Laboratories) in combination with green fluorescent Alexa Fluor 488 goat anti-mouse antibody (Invitrogen, Germany). Thereafter, sections were washed with PBS, and the nuclei stained bright blue with 4′-6-diamidino-2-phenylindole (DAPI) (0.1 μg/ml in PBS) (Sigma).

3.2. Quantification of Immunostaining. The method of quantification of colocalization of mitochondria with cytochrome C in the kidney has been described in detail elsewhere [25, 26]. Briefly, quantification of immunofluorescent colocalization of mitochondrial marker with cytochrome C in kidney tissue sections was performed by using the Zeiss Zen 2009 software Carl Zeiss Micro-Imaging GmbH (Göttingen, Germany). Colocalization of proteins of interest was quantified by calculating the colocalization coefficient as derived from Mander's article based on Pearson's correlation coefficient [26]. Images were adjusted to a threshold to exclude background fluorescence and gated to include intensity measurements only from positively stained cells. The number of caspase-3-stained nuclei was determined by the formula: caspase-3-stained nuclei/total number of DAPI-stained nuclei × 100. For image analysis, using the area of the whole stained tissue section, five rats per group were used for analysis. Data were expressed as means ± SEM.

3.3. Statistical Analysis. All tests were performed using SPSS 20.0 software program. Normal distribution was analyzed with the Kolmogorov-Smirnov test. The results are expressed as means ± SEM. Statistical significance between the two groups was analyzed by the Student t-test or Mann–Whitney test as appropriate. $p < 0.05$ was considered statistically significant. All tests were performed using Sigma Plot 13.0 statistical software.

4. Results

4.1. Increased Heart and Lung Weight Indices following Congestive Heart Failure. Body weights of rats with ACF-induced heart failure were not significantly different from sham-operated controls (Figure 1). In contrast, the heart and lung weight indices were significantly increased at 28 ± 2 days after ACF-induced heart failure ($p < 0.01$) (Figure 1).

4.2. Systolic and Diastolic Dysfunction in ACF Rats. In vivo hemodynamic measurements of control and ACF rats showed that central venous (CVP) and left end-diastolic pressure (LVEDP) were significantly increased in ACF rats ($p < 0.01$) (Table 1). While the left ventricular end-diastolic and end-systolic volumes (LVEDV and LVESV, resp.) were significantly elevated ($p < 0.01$), the left ventricular ejection fraction (LVEF) ($p < 0.01$), and the maximum rate of pressure development ($p < 0.01$) were significantly reduced (Table 1).

4.3. Histopathological Changes in the Kidney following Congestive Heart Failure. In kidney tissue sections of control rats, a normal structure of glomeruli as well as proximal and distal tubuli was observed (Figures 2(a) and 2(b)). In contrast, kidney sections of ACF rats showed signs of morphological and pathological changes (Figures 2(c) and 2(d)). In the glomerular region of the kidney, several glomeruli showed atrophic changes, widening of Bowman's space with obvious degeneration of cells and losing the prominent glomerular structure suggesting apoptotic cell death. As compared to controls (Figures 2(a) and 2(b)), the proximal convoluted tubuli in ACF animals showed atrophic changes including epithelial shedding and loss of brush border (Figures 2(c) and 2(d)). Furthermore, pyknotic nuclei and desquamated cells (Figure 2) were seen in the tubular region. Tubular lumen was found to be sometimes obliterated due to degeneration and swelling of lining epithelial cells. The distal kidney tubuli of ACF rats revealed signs of degeneration, manifested by desquamation of epithelial tubular cells (Figure 2).

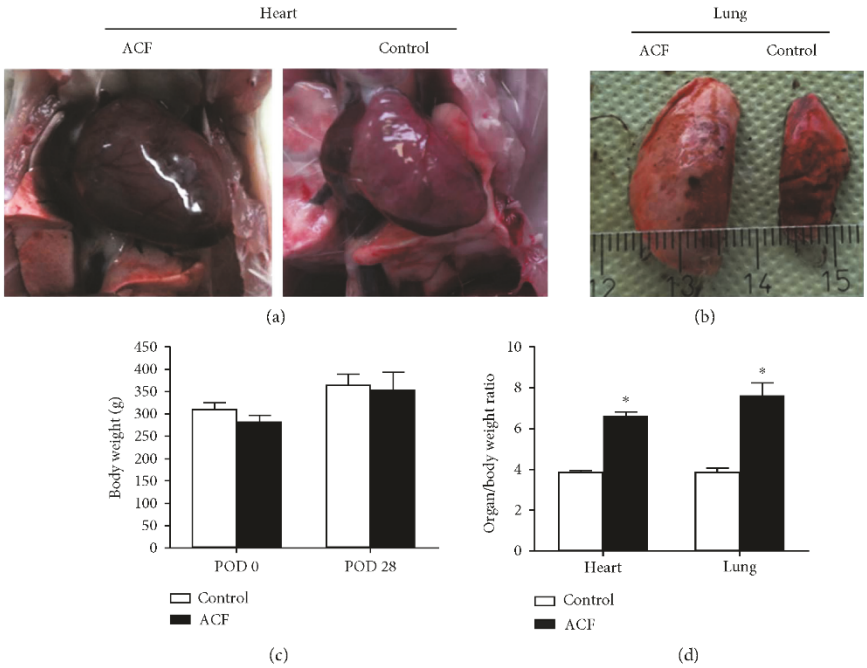

FIGURE 1: (a) and (b) show the enlarged size of the heart (a) and lung (b) in rats with ACF-induced heart failure compared to sham-operated controls. These animals revealed significantly increased heart and lung weight indices (d), but not body weight. (c) * denotes significant differences compared to control ($p < 0.01$, Student t-test).

TABLE 1: Hemodynamic parameters.

	Control ($n = 5$)	ACF ($n = 5$)
SV (μl)	$134 \pm 3^*$	$298 \pm 40^*$
LVEF (%)	$74 \pm 2^*$	$45 \pm 4^*$
LVEDP (mmHg)	$5.1 \pm 0.3^*$	$12.1 \pm 1^*$
ZVD (mmHg)	$0.1 \pm 0.1^*$	$5.6 \pm 1^*$
HR (min^{-1})	$340.41 \pm 10^+$	$316.98 \pm 10^+$
LVESV (μl)	$48.18 \pm 5^*$	$359.71 \pm 36^*$
LVEDV (μl)	$181.86 \pm 8^*$	$658.04 \pm 61^*$

$^*p < 0.05$. + indicates $p = 0.717$.

5. Detection of DNA Fragmentation by Tunel Staining in Kidney Cells following Congestive Heart Failure

Apoptosis was confirmed by TUNEL staining. In ACF kidneys, apoptosis was observed by TUNEL staining predominantly in tubular epithelial cells. Both proximal and distal tubule cells displayed DAPI-positive nuclei that were intensely TUNEL positive (Figures 3(b) and 3(f)). Furthermore, TUNEL-positive cells were not present in controls (Figures 3(a) and 3(e)).

5.1. Expression of Proapoptotic Bax in Kidney Cells following Congestive Heart Failure. To corroborate the TUNEL findings and to investigate the possible mechanisms mediating kidney apoptosis, we measured apoptotic factors in the kidney following ACF-induced heart failure. Examining kidney tissue of control rats by immunofluorescence confocal microscopy, proapoptotic Bax immunostaining was faintly observed in the proximal and distal tubuli; however, no staining was found in the glomeruli or interstitium (Figures 3(c) and 3(g)). After the induction of ACF-induced heart failure, overt Bax staining was noticeable in the damaged proximal and distal tubular cells of kidney tissue sections (Figures 3(d) and 3(h)). Also, some glomerular cells showed positive staining (Figures 3(d) and 3(h)).

5.2. Mitochondrial Leakage of Cytochrome C into the Cytosol of Kidney Cells following Congestive Heart Failure. In kidney tissue sections of control rats, cytochrome C immunoreactivity was localized primarily to mitochondria as indicated by an almost complete overlap with the mitochondrial marker within renal tubular cells (Figure 4). In contrast, cytochrome C immunofluorescence was found primarily within the cytoplasm especially in perinuclear area of renal tubular cells after heart failure induction, where it no longer colocalized with mitochondrial marker (Figure 4). Quantification of the colocalization coefficient of cytochrome C and mitochondrial

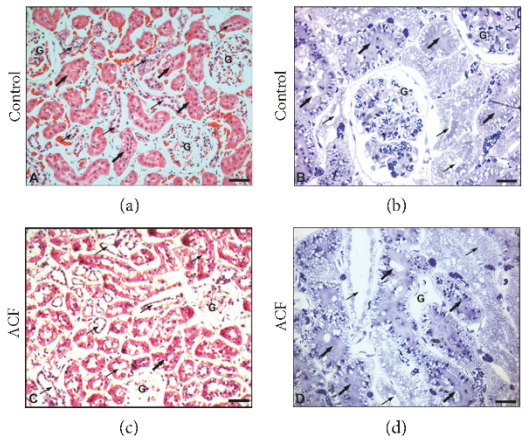

FIGURE 2: Light microscopic photographs of representative kidney sections of control and ACF adult rats. (a) and (b) show control haematoxylin-eosin- (a) and toluidine blue-stained (b) rat kidney with normal distal (thin arrow), proximal (thick arrow) tubular and glomerulus (G) structures are seen in the medulla of control kidney. (c) and (d) show ACF haematoxylin-eosin- (c) and toluidine blue-stained (d) rat kidney with histopathological changes in atrophic glomeruli (G) with atrophic changes such as widening of Bowman's space with haemolysis, necrosis with obvious degeneration in nuclei, and apoptotic cell death. Also, histopathological changes in atrophic distal (thin arrow) and proximal (thick arrow) tubular structures are shown with epithelial shedding and loss of brush border of proximal tubules as well as desquamation of tubular epithelium of distal tubules in the medulla. (a), (c): ×120; (b), (d): ×200.

marker within kidney sections showed a significant reduction of their colocalization in ACF animals compared to controls (Figure 5(a)) indicating that cytochrome C had leaked from mitochondria into the cytoplasm.

5.3. Nuclear Transfer of Caspase-3 as Activated Caspase-3 into the Nucleus of Kidney Cells following Congestive Heart Failure. We evaluated the localization of caspase-3 using antibodies that detect cleaved caspase-3-recombinant protein alone or with pro-caspase-3-recombinant proteins in kidney sections by confocal immunofluorescence microscopy in ACF and sham-operated control rats (Figure 6). Immunofluorescence confocal microscopy of kidney sections of control rats revealed that caspase-3 immunoreactivity was confined primarily to well-defined subcellular structures in proximal and distal tubular cells of the kidney, no staining was found in the glomeruli or interstitium. In contrast, caspase-3 immunofluorescence was translocated into perinuclear area of cells or nuclei within tubular cells in ACF rats. Also, some glomerular cells show positive staining (Figure 6) indicating that caspase-3 translocated in the active form. Therefore, we used the apoptotic marker cleaved activated caspase-3 which is absent under normal conditions and detectable only during cell apoptosis. Indeed, using an antibody which detects cleaved caspase-3-recombinant protein in kidney sections of ACF rats revealed that cleaved caspase-3 immunoreactivity was confined primarily to perinuclear area of cells or nuclei within tubular cells (Figure 6(b)).

Importantly, the number of caspase-3-IR nuclei as well as cleaved caspase-3-IR nuclei cells in relation to the total number of DAPI-stained nuclei was significantly higher in ACF rats than in controls ($p < 0.05$) (Figure 6(b)).

5.4. Transmission Electron Microscopy Evaluation of Kidney Cells following Congestive Heart Failure. Ultrastructural examination of kidney from control rats contrasted with uranyl acetate and lead citrate presents normal tissue of kidney ultrastructure containing mitochondria and endoplasmic reticulum (Figure 7(a)). In contrast, kidney sections from ACF rats present a marked cytoplasmic vacuolization of cells and dilated endoplasmic reticulum, mitochondria, and pleomorphic lysosomes containing flocculent material. In addition, the changes in the structure of renal glomeruli and tubular cells of ACF kidney included signs of matrix vacuolization, dilation of capillary, and degeneration of cell nuclei. In edematous regions, the space between individual tubuli was enlarged and there was a marked capillary dilation in the peritubular area (Figure 7(b)). The morphology of the renal tubules was also affected as reflected with numerous swollen mitochondria with a crista disarrangement and partial cristolysis within tubular epithelium (Figure 7(c)).

6. Discussion

Progressive heart failure is associated with growing deterioration of kidney function which in turn leads to a hemodynamic and neurohumoral worsening of heart failure, thereby, increasing the risk of mortality by 7.5-fold [1]. This study investigated the possible mechanisms that underlie renal damage following heart dysfunction using the rat model of infrarenal aortocaval fistula-induced heart failure. Kidney tissue sections of these animals showed light microscopic alterations such as congestion, glomerular atrophy with widening of Bowman's space, edema with epithelial shedding in tubular structures, pyknotic nuclei,

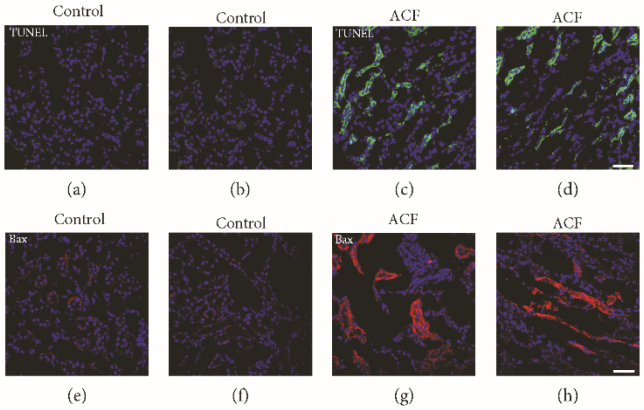

FIGURE 3: Confocal microscopy of TUNEL staining ((a), (b), (c), and (d)) and proapoptotic Bax ((e), (f), (g), and (h)) in the kidney of control and ACF adult rats. (a), (b), (c), and (d) showed TUNEL-positive (green fluorescence) with DAPI-counterstained nucleus (blue fluorescence) immunofluorescence of the kidney in control or ACF adult rats. Note that apoptotic tubular cells were detected in the kidney following ACF-induced heart failure in rats (c) and (d); however, no staining was found in controls (a) and (b). (e), (f), (g), and (h) Confocal microscopy of proapoptotic Bax protein (red fluorescence) with DAPI-counterstained nucleus (blue fluorescence) immunofluorescence in the kidney in control or in ACF adult rats. Note that the absence or weak Bax immunostaining was detected in the renal tubular cell cytoplasm of control kidney (e) and (f). However, strong positive immunofluorescence staining within renal tubular cell cytoplasm after heart failure induction was detected (g) and (h). Bar = 20 μm.

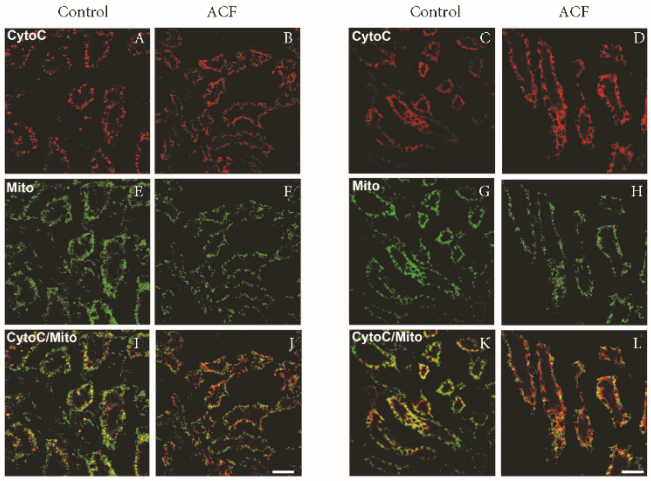

FIGURE 4: Confocal microscopy of cytochrome C (red fluorescence) with mitochondrial marker (green fluorescence) double immunofluorescence of the renal tubular cells in the kidney of control and ACF adult rats. Note that the cytochrome C immunostaining overlapped with the mitochondrial marker in the cytoplasm of renal tubular cells of control kidney (A, E, I and C, G, K). However, cytochrome C immunofluorescence was confined primarily within the cytoplasm after heart failure induction, where it no longer colocalized with mitochondria within renal tubular cells (B, E, J and D, H, L). Bar = 20 μm.

desquamated cells, and hemorrhages suggesting apoptotic events. Consistently, double immunofluorescent staining revealed enhanced expression of proapoptotic Bax, mitochondrial leakage of cytochrome C, and nuclear transfer of activated caspase-3 indicating apoptotic processes. Finally, electron microscopy confirmed the presence of apoptosis by signs of nuclear condensation, DNA fragmentation, shrinkage, and dissolution of the mitochondrial structure. These

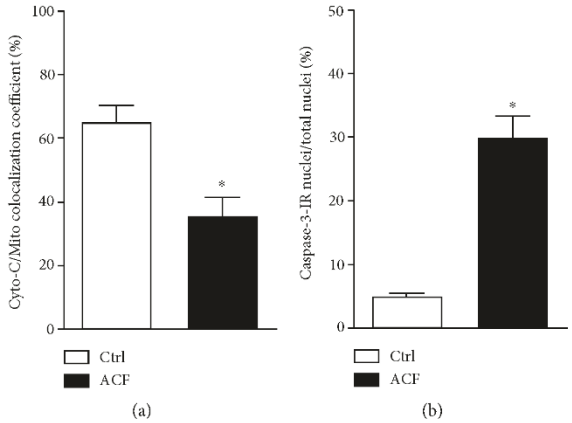

FIGURE 5: (a) Quantitative analysis of immunofluorescence microscopy of mitochondrial leakage of cytochrome C into the cytosol as well as nuclear transfer of caspase-3 as activated caspase-3 into the nucleus of kidney cells following congestive heart failure. Quantitative analysis of immunofluorescence microscopy of the colocalization coefficient of cytochrome C and mitochondrial marker showing a significant reduction of their colocalization in the liver in ACF animals compared to in controls ($n = 5$, $p < 0.05$, Student t-test). (b) Quantitative analysis of immunofluorescence microscopy for cleaved caspase-3-IR renal tubular cell nuclei in the kidney of ACF animals relative to the control (* denotes significant differences compared to control, $n = 5$, $p < 0.05$, Student t-test).

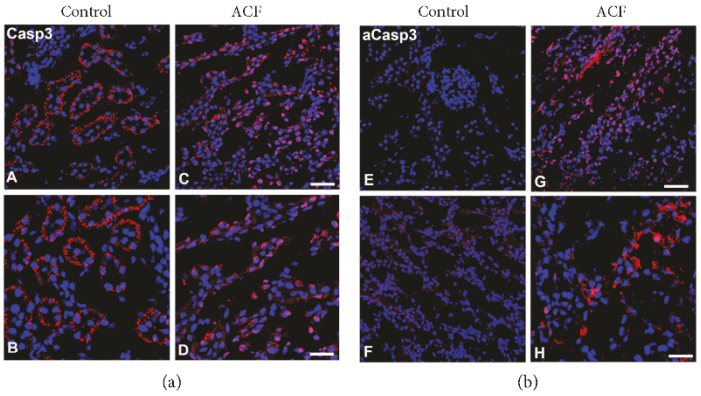

FIGURE 6: Confocal immunofluorescence microscopy of caspase-3 (red fluorescence) using an antibody detecting pro-caspase-3 recombinant protein (A–D) or cleaved caspase-3-recombinant protein (E–H) with DAPI-counterstained nuclei (blue fluorescence) in the kidney sections of control or ACF adult rats. (A–D) Note that caspase-3 immunoreactivity was confined primarily to well-defined subcellular organelles like structures in renal tubular cells within the kidney in control rats. In contrast in ACF rats, caspase-3 immunofluorescence was transferred into the perinuclear area of cells or inside the nuclei of renal tubular cells (C and D) indicating an activation of proapoptotic factor caspase-3. (E–H) Confocal immunofluorescence microscopy caspase-3 (red fluorescence) and DAPI-counterstained nuclei (blue fluorescence) in kidney sections using an antibody detecting exclusively cleaved caspase-3-recombinant protein. (G and H) showed that cleaved caspase-3 immunoreactivity was confined primarily to perinuclear area of cells or nuclei within renal tubular cells of ACF rat kidney (D); however, no staining was found in the control (F). Bar = 20 μm.

findings provide morphological evidence of apoptotic events during kidney injury resulting from congestive heart failure.

Recently, our group successfully modified an experimental model of heart failure by the induction of an infrarenal aortocaval fistula which resulted in overt signs of congestive heart failure within a predictable short-time period [17]. Heart performance and kidney function are closely interconnected, and a close link exists between these organs [1]. Dysfunction of one organ often leads to a deterioration of function of the other one such as the kidney [27]. Recently,

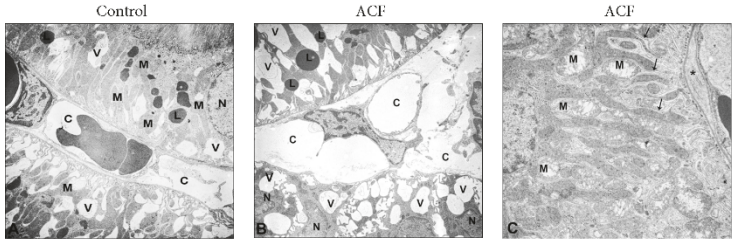

FIGURE 7: Transmission electron micrograph of the rat kidney in control (a) and ACF (b and c) groups. (a) shows normal ultrastructure of the control kidney. Note; untreated control of kidney cells consist of vital nucleus (N), well-developed cell organelles like mitochondria (M), lysosome (L), and a well-organized cytoplasm. (b) Electron microscopic demonstration of the ACF kidney tissue. Note that ultrastructure evaluations show a marked cytoplasmic vacuolization (V) of cells and capillary (C) dilation in the peritubular area and dilated cell organelles and cell nuclei (N) became condensed indicating intrinsic apoptotic events. (c) Many swollen mitochondria situated between the extensive inholdings (arrow) of the basolateral plasma membrane (*) that create the lateral cell processes of distal tubules become dilated and exhibit a crista disarrangement and partial cristolysis. ×5000; bars:1 μm.

the investigation of organ crosstalk in acute renal injury reported that cell death, inflammation, cytokine and chemokine overexpression, caspase-mediated apoptotic mechanisms, and oxidative stress might induce distant organ dysfunction [28, 29]. Consistently, the progression of heart failure may contribute to gradual toxic injury to renal cells including apoptosis and consequently persistent kidney damage and functional loss [5, 9]. Therefore, we investigated pathological changes in the kidney following ACF-induced heart failure in rats. Our histological investigation revealed that the glomeruli and tubuli in the kidneys of heart failure rats showed morphological and pathological changes such as mitochondrial condensation and nuclear degeneration suggesting apoptotic cell death as compared to controls. Consistently, kidney apoptosis was observed by TUNEL staining as reflected with TUNEL-positive apoptotic tubular cells in the kidney following ACF-induced heart failure. Our findings are in agreement with a previous study showing that the microvascular endothelial permeability, inflammation, and tubular cell apoptosis significantly increased in rat kidneys following left coronary artery-induced myocardial infarction [11].

Then, we further corroborated evidence for apoptotic events by demonstrating increased expression of the proapoptotic protein Bax in renal tubule epithelial cells and glomeruli after heart failure induction. Our findings are in agreement with the previous report by Yang et al., [30] showing that Bax overexpression positively correlated with caspase-3 activity and subsequent renal apoptosis that was associated with renal inflammation, tubular atrophy, and renal fibrosis in experimental glomerulonephritis. Recent evidence is emerging that the mitochondria-mediated apoptosis is initiated by a variety of apoptosis-inducing signals that cause the imbalance of the major apoptosis regulator such as Bax [15]. Indeed, the previous studies reported that the proapoptotic protein Bax after being activated triggers the disruption of mitochondrial transmembrane potential, followed by mitochondrial swelling and an increase in the permeability of the outer mitochondrial membrane [12–14]. Therefore, we extended our investigation to determine the apoptotic pathway-mediated mitochondrial enzyme cytochrome C in renal cell death during heart failure. Indeed, our immunofluorescence confocal microscopy revealed that cytochrome C immunoreactivity was confined primarily to mitochondria within renal tubule epithelial cells in control rats; however, it leaked into the cytosol of renal tubule epithelial cells following heart failure, where it no longer colocalized with mitochondria. This is in agreement with previous studies reporting that cytochrome C released from mitochondria to the cytosol initiates caspase activation in isolated kidney cortex after cadmium-induced apoptosis [31]. Similarly, another previous study reported that cytochrome C is released from mitochondria to the cytosol during apoptotic events such as hypertensive nephrosclerosis in rats [32].

We further corroborated the evidence for apoptotic pathway-mediated renal cell death by providing further morphological evidence for the activation of caspase-3 from cell organelles like structures that could be shown to translocate in the cleaved form into the perinuclear area of renal tubule epithelial and glomerular cells after heart failure. Our results receive good support from previous studies demonstrating the activation of caspase-3 in cisplatin-induced renal injuries [33] as well as in polymyxin-induced apoptosis in rat kidney proximal tubular cells [34].

In summary, heart failure often leads to the damage of the kidneys, a phenomenon called cardiorenal syndrome [9]. Our present study demonstrates that progressive heart failure [21] is associated with obvious apoptotic events with nucleus degeneration, mitochondrial swelling, and cell death in the glomerular and tubular area of the kidney. In parallel, under normal conditions, cytochrome C colocalized primarily with cell mitochondria and cleaved caspase-3 was absent. In heart failure, the overexpression of proapoptotic Bax protein concomitant with cytochrome C released from the outer mitochondrial membrane into cell cytoplasm led to subsequent caspase-3 activation triggering apoptotic events. These findings provide morphological evidence of renal injury resulting from congestive heart failure and support the pathological interactions between the heart and kidney during heart failure.

Conflicts of Interest

The authors declare that they have no conflicts of interest.

Authors' Contributions

All authors have contributed to the design and execution of the study.

Acknowledgments

The authors thank Claudia Spies, M.D. (director and professor, Department of Anesthesiology and Intensive Care Medicine, Charité University Berlin, Germany), for her continuous support and Mrs. Petra von Kwiatkowski and Susanne Runewitz (technician, Berlin, Germany), for their technical assistance. Doaa M. Mohamed is supported by a scholarship from the Faculty of Science at Aswan University and the Egyptian Government.

References

[1] G. C. Fonarow, K. F. Adams Jr., W. T. Abraham, C. W. Yancy, W. J. Boscardin, and ADHERE Scientific Advisory Committee, Study Group, and Investigators, "Risk stratification for in-hospital mortality in acutely decompensated heart failure: classification and regression tree analysis," *JAMA*, vol. 293, no. 5, pp. 572–580, 2005.

[2] L. A. Allen, G. M. Felker, S. Pocock et al., "Liver function abnormalities and outcome in patients with chronic heart failure: data from the candesartan in heart failure: assessment of reduction in mortality and morbidity (CHARM) program," *European Journal of Heart Failure*, vol. 11, no. 2, pp. 170–177, 2009.

[3] R. de Silva, A. S. Rigby, K. K. Witte et al., "Anemia, renal dysfunction, and their interaction in patients with chronic heart failure," *The American Journal of Cardiology*, vol. 98, no. 3, pp. 391–398, 2006.

[4] K. Damman, G. Navis, A. A. Voors et al., "Worsening renal function and prognosis in heart failure: systematic review and meta-analysis," *Journal of Cardiac Failure*, vol. 13, no. 8, pp. 599–608, 2007.

[5] C. Ronco, A. A. House, and M. Haapio, "Cardiorenal syndrome: refining the definition of a complex symbiosis gone wrong," *Intensive Care Medicine*, vol. 34, no. 5, pp. 957–962, 2008.

[6] P. A. McCullough, S. Steigerwalt, K. Tolia et al., "Cardiovascular disease in chronic kidney disease: data from the Kidney Early Evaluation Program (KEEP)," *Current Diabetes Reports*, vol. 11, no. 1, pp. 47–55, 2011.

[7] A. Goldberg, H. Hammerman, S. Petcherski et al., "Inhospital and 1-year mortality of patients who develop worsening renal function following acute ST-elevation myocardial infarction," *American Heart Journal*, vol. 150, no. 2, pp. 330–337, 2005.

[8] J. T. Heywood, "The cardiorenal syndrome: lessons from the ADHERE database and treatment options," *Heart Failure Reviews*, vol. 9, no. 3, pp. 195–201, 2004.

[9] L. G. Bongartz, M. J. Cramer, P. A. Doevendans, J. A. Joles, and B. Braam, "The severe cardiorenal syndrome: 'Guyton revisited'," *European Heart Journal*, vol. 26, no. 1, pp. 11–17, 2005.

[10] C. Y. Goh, G. Vizzi, M. De Cal, and C. Ronco, "Cardiorenal syndrome: a complex series of combined heart/kidney disorders," *Contributions to Nephrology*, vol. 174, pp. 33–45, 2011.

[11] E. Cho, M. Kim, Y. S. Ko et al., "Role of inflammation in the pathogenesis of cardiorenal syndrome in a rat myocardial infarction model," *Nephrology, Dialysis, Transplantation*, vol. 28, no. 11, pp. 2766–2778, 2013.

[12] D. R. Green, "Apoptotic pathways: paper wraps stone blunts scissors," *Cell*, vol. 102, no. 1, pp. 1–4, 2000.

[13] I. Budihardjo, H. Oliver, M. Lutter, X. Luo, and X. Wang, "Biochemical pathways of caspase activation during apoptosis," *Annual Review of Cell and Developmental Biology*, vol. 15, pp. 269–290, 1999.

[14] J. Deng, G. Wang, Q. Huang et al., "Oxidative stress-induced leaky sarcoplasmic reticulum underlying acute heart failure in severe burn trauma," *Free Radical Biology & Medicine*, vol. 44, no. 3, pp. 375–385, 2008.

[15] Y. Guo, W. Zhang, Y. Y. Yan et al., "Triterpenoid pristimerin induced HepG2 cells apoptosis through ROS-mediated mitochondrial dysfunction," *Journal of BUON*, vol. 18, no. 2, pp. 477–485, 2013.

[16] R. Garcia and S. Diebold, "Simple, rapid, and effective method of producing aortocaval shunts in the rat," *Cardiovascular Research*, vol. 24, no. 5, pp. 430–432, 1990.

[17] S. Treskatsch, A. Feldheiser, A. T. Rosin et al., "A modified approach to induce predictable congestive heart failure by volume overload in rats," *PLoS One*, vol. 9, no. 1, article e87531, 2014.

[18] M. R. Dent, P. S. Tappia, and N. S. Dhalla, "Gender differences in cardiac dysfunction and remodeling due to volume overload," *Journal of Cardiac Failure*, vol. 16, no. 5, pp. 439–449, 2010.

[19] P. Pacher, T. Nagayama, P. Mukhopadhyay, S. Bátkai, and D. A. Kass, "Measurement of cardiac function using pressure-volume conductance catheter technique in mice and rats," *Nature Protocols*, vol. 3, no. 9, pp. 1422–1434, 2008.

[20] D. C. Saha, A. C. Saha, G. Malik, M. E. Astiz, and E. C. Rackow, "Comparison of cardiovascular effects of tiletamine-zolazepam, pentobarbital, and ketamine-xylazine in male rats," *Journal of the American Association for Laboratory Animal Science*, vol. 46, no. 2, pp. 74–80, 2007.

[21] S. Treskatsch, M. Shakibaei, A. Feldheiser et al., "Ultrastructural changes associated with myocardial apoptosis, in failing rat hearts induced by volume overload," *International Journal of Cardiology*, vol. 197, pp. 327–332, 2015.

[22] P. Mayer, "Ueber das Faerben mit Haematoxylin," *Mittheilungen aus der Zoologischen Station zu Neapal*, vol. 10, no. 10, pp. 170–186, 1981.

[23] S. A. Mousa, M. Shakibaei, N. Sitte, M. Schäfer, and C. Stein, "Subcellular pathways of beta-endorphin synthesis, processing, and release from immunocytes in inflammatory pain," *Endocrinology*, vol. 145, no. 3, pp. 1331–1341, 2004.

[24] S. A. Mousa, M. Shaqura, J. Winkler et al., "Protein kinase C-mediated mu-opioid receptor phosphorylation and desensitization in rats, and its prevention during early diabetes," *Pain*, vol. 157, no. 4, pp. 910–921, 2016.

[25] M. Shaqura, X. Li, M. Al-Khrasani et al., "Membrane-bound glucocorticoid receptors on distinct nociceptive neurons as potential targets for pain control through rapid non-genomic effects," *Neuropharmacology*, vol. 111, pp. 1–13, 2016.

[26] E. M. Manders, F. J. Verbeek, and J. A. Aten, "Measurement of colocalization of objects in dual-color confocal images," *Journal of Microscopy Oxford*, vol. 169, pp. 375–382, 1993.

[27] C. W. Yancy, M. Jessup, B. Bozkurt et al., "2013 ACCF/AHA guideline for the management of heart failure: a report of the American College of Cardiology Foundation/American Heart Association Task Force on Practice Guidelines," *Journal of the American College of Cardiology*, vol. 62, no. 16, pp. e147–e239, 2013.

[28] C. P. Li, J. H. Li, S. Y. He, P. Li, and X. L. Zhong, "Roles of Fas/Fasl, Bcl-2/Bax, and caspase-8 in rat nonalcoholic fatty liver disease pathogenesis," *Genetics and Molecular Research*, vol. 13, no. 2, pp. 3991–3999, 2014.

[29] B. Bang, R. Gniadecki, and B. Gajkowska, "Disruption of lipid rafts causes apoptotic cell death in HaCaT keratinocytes," *Experimental Dermatology*, vol. 14, no. 4, pp. 266–272, 2005.

[30] F. Yang, Y. H. Liu, X. P. Yang, J. Xu, A. Kapke, and O. A. Carretero, "Myocardial infarction and cardiac remodelling in mice," *Experimental Physiology*, vol. 87, no. 5, pp. 547–555, 2002.

[31] W. K. Lee, U. Bork, and F. Thevenod, "Mitochondria as a target of cadmium nephrotoxicity: induction of swelling and cytochrome C release," *Toxicology Mechanisms and Methods*, vol. 14, no. 1-2, pp. 67–71, 2004.

[32] W. Z. Ying and P. W. Sanders, "Cytochrome c mediates apoptosis in hypertensive nephrosclerosis in Dahl/Rapp rats," *Kidney International*, vol. 59, no. 2, pp. 662–672, 2001.

[33] G. P. Kaushal, V. Kaushal, X. Hong, and S. V. Shah, "Role and regulation of activation of caspases in cisplatin-induced injury to renal tubular epithelial cells," *Kidney International*, vol. 60, no. 5, pp. 1726–1736, 2001.

[34] M. A. Azad, J. Akter, K. L. Rogers, R. L. Nation, T. Velkov, and J. Li, "Major pathways of polymyxin-induced apoptosis in rat kidney proximal tubular cells," *Antimicrobial Agents and Chemotherapy*, vol. 59, no. 4, pp. 2136–2143, 2015.

10. Affidavit

I, Noureddin B. Aboryag, certify under penalty of perjury by my own signature that I have submitted the thesis on the topic **[Stress-induced alterations in the organ systems during heart failure following an aortocaval fistula in rats].** I wrote this thesis independently and without assistance from third parties, I used no other aids than the listed sources and resources.

All points based literally or in spirit on publications or presentations of other authors are, such as, in proper citations (see "uniform requirements for manuscripts (URM)" the ICMJE www.icmje.org) indicated. The sections on methodology (in particular practical work, laboratory requirements, statistical processing) and results (in particular images, graphics and tables) correspond to the URM (s.o) and are answered by me. My contributions in the selected publications for this dissertation correspond to those that are specified in the following joint declaration with the responsible person and supervisor. All publications resulting from this thesis and which I am author of correspond to the URM (see above) and I am solely responsible.

The importance of this affidavit and the criminal consequences of a false affidavit (section 156,161 of the Criminal Code) are known to me and I understand the rights and responsibilities stated therein.

Date:

Noureddin B. Aboryag

12. Curriculum Vitae

"Mein Lebenslauf wird aus datenschutzrechtlichen Gründen in der elektronischen Version meiner Arbeit nicht veröffentlicht."

13. Publications

- **Aboryag** NB**,** Mohamed DM, Dehe L, Shaqura M, Treskatsch S, Shakibaei M, Schäfer M, Mousa SA. Histopathological Changes in the Kidney following Congestive Heart Failure by Volume Overload in Rats. Oxid Med Cell Longev, 2017; 2017: 6894040. https://doi.org/10.1155/2017/6894040. (IF: 4.936).

- Shaqura M, Mohamed DM, **Aboryag NB**, Bedewi L, Dehe L, Treskatsch S, Shakibaei M, Schäfer M, Mousa SA. Pathological alterations in liver injury following congestive heart failure induced by volume overload in rats. PLoS ONE, 2017; 12(9): e0184161. https://doi.org/10.1371/journal.pone.0184161. (IF: 2.806)

14. Acknowledgement

I would like here to give my special thanks to my supervisor **Prof. Dr. med. Michael Schäfer** who supported me during the whole process of my doctoral thesis and introduced me to a new exciting field of research, Histopathology. Additionally, I am also very grateful for his friendly behavior and great help. In this context, I would also like to give my special thanks to **Dr. Shaaban Mousa**, as co-supervisor, he was always helpful, friendly in answering all questions and overall was interested in my work in particular in immunohistochemistry. During my years in the Schäfer group, **Dr. Mohammed Shaqura** helped me with all scientific and technical questions that I had and taught me several helpful operation techniques. Furthermore, I want to thank all the other laboratory members: Petra von Kwiatkowski, Susana Runewitz, who were always helpful and nice to me and had to endure my special kind of humor as well as the times when I was overexcited or on the wrong track. Apart from work, I would like to thank my family, who gave me the opportunity to study the field of my interest and supported me when they know that I had found my goal. My wife, the best women in the world, thanks too much for your support and your hard patience and endurance during my study when I was far away from you. My sons AL Bashir and Mazen, thanks a lot for your patience and endurance. Thanks very much to my country for supporting me.